A constant influx model for dike propagation: implications for magma reservoir dynamics

Paola Traversa, V. Pinel, J. -R. Grasso

A Constant Influx Model for Dyke Propagation. Implications for Magma Reservoir Dynamics

P. Traversa,[1] V. Pinel,[2] and J.R. Grasso,[1]

J.R. Grasso, LGIT - CNRS - OSUG - Université Joseph Fourier BP 53 38041 Grenoble Cedex 9, France.

V. Pinel, LGIT - CNRS - IRD - Université de Savoie, Campus Scientifique, 73376 Le Bourget du Lac Cedex, France.

P. Traversa, LGIT - CNRS - OSUG - Université Joseph Fourier BP 53 38041 Grenoble Cedex 9, France. (paola.traversa@obs.ujf-grenoble.fr)

[1]Laboratoire de Géophysique Interne et Tectonophysique, CNRS, Université Joseph Fourier, BP 53 38041 Grenoble Cedex 9, France.

[2]Laboratoire de Géophysique Interne et Tectonophysique, CNRS, IRD, Université de Savoie, Campus Scientifique, 73376 Le Bourget du Lac Cedex, France.

Abstract. Most observations of seismicity rate during dyke propagation on basaltic volcanoes show: (i) rate stationarity despite possible variations of the dyke tip velocity, (ii) frequent lack of clear and monotonic hypocenter migration following dyke propagation, (iii) event occurrences located backwards with respect to the dyke tip position. On these bases, the origin of the seismicity contemporary to dyke intrusion within basaltic volcanoes cannot be solely related to the crack-tip propagation. Seismicity rather appears to be the response of the edifice itself to the volumetric deformation induced by the magma intruding the solid matrix. This in the unit time being the flux of magma entering the fracture, it argues for the stationary seismicity rate accompanying the intrusion to be a proxy for a constant magma supply rate from the magma reservoir. We consider a two-phase dyke propagation model, including a first vertical propagation followed by a lateral migration along a lithological discontinuity. We explore (i) under which geophysical conditions the vertical dyke is fed at constant flow rate of magma and (ii) dyke propagation patterns. Implications entailed by constant volumetric flux on the Piton de la Fournaise volcano case study suggest a minimum size for the magma reservoir of about 1 km^3, and a maximum value for the initial magma reservoir overpressure of about 2.2 MPa. Considering similar magma inflow rates during vertical and lateral dyke propagation phases, we reproduce independent estimates of propagation velocities, rising times and injected volumes when applying the model to the August 2003 Piton de la Fournaise eruption.

1. Introduction

Magma-driven fracture is a commonly observed mechanism that allows to rapidly transport melt through cold and brittle country rock without extensive solidification [*Lister and Kerr*, 1991]. It therefore differs from porous flow through a deformable and partially molten matrix, which is characteristic of melt generation in the mantle [e.g. *McKenzie*, 1984] and from slow diapiric rise of granite through viscous country rock [*Pitcher*, 1979; *Rubin*, 1993a].

The difficulty of making direct observations of the plumbing system and of the dynamics of conduit formation within volcanoes makes only approximate the knowledge of the parameters and physical balances that govern the propagation of the fissure system.

Previous authors have proposed analytical models of fluid-driven fracture [e.g. *Lister*, 1990a, b; *Lister and Kerr*, 1991; *Roper and Lister*, 2005]. These studies suppose that dykes are fed from a reservoir of magma at depth; the crack is initiated within the chamber walls, where favorable conditions promote dyke propagation, leading to magmatic injections.

The competing pressures, whose balance drives the dyke propagation, are: (i) the elastic stresses generated by deformation of the host rock; (ii) the stresses required to extend the tip against the rock resistance; (iii) the buoyancy forces related to the difference between magma and country rock densities; (iv) the viscous pressure drop due to magma flow; (v) the magma driving overpressure; and (vi) the regional pre-existing stressfield [e.g. *Lister*,

1990b; *Lister and Kerr*, 1991]. In this framework *Lister* [1990a] concludes that the fracture mechanics only characterise the crack tip zone, while the crack width and the rate of crack propagation are determined by the fluid dynamics. Static or quasi-static solutions for equilibrium crack are therefore inappropriate. It follows that the most important role in the pressure balances is played by (i), (iii), (iv) and (v). Note that (ii) is negligible "soon" away from the crack tip, and (vi) mainly acts on the dyke orientation [*Lister*, 1990b; *Lister and Kerr*, 1991].

In the literature, dyke propagation has been modeled according to two basic independent boundary conditions. On one hand some authors consider the fluid fracture as driven by a constant overpressure magma chamber at its base [*Rubin*, 1993b, a; *Meriaux and Jaupart*, 1998; *Roper and Lister*, 2005]. On the other hand *Lister* [1990a, b] assume a constant influx condition. The first hypothesis has been claimed geologically more appropriate than the second one [e.g. *Meriaux and Jaupart*, 1998]. The dyke growth model from a finite size magma chamber proposed by *Ida* [1999], however, leads the author to conclude that only in the case of extremely large and compressible magma reservoirs the melt pressure is actually able to remain constant as the dyke propagates.

From the observation point of view, we only have indirect access to dyke propagation, the only parameter we can estimate being the propagation velocity, i.e. few meters per second on basaltic volcanoes. These velocities can be deduced either from observations of the seismic signals associated with

the advancing crack tip [*Aki et al.*, 1977; *Shaw*, 1980; *Battaglia et al.*, 2005], or inferred from the size and composition of xenolithes carried by the flow [*Carmichael et al.*, 1977; *Spera*, 1980; *Pasteris*, 1984], or inferred from surface deformation measurements [e.g. *Toutain et al.*, 1992; *Battaglia and Aki*, 2003; *Peltier et al.*, 2005; *Aloisi et al.*, 2006; *Peltier et al.*, 2007]. As pointed by *Battaglia et al.* [2005] and *Klein et al.* [1987], however, well-documented cases of earthquake hypocenters migrating simultaneously to the injected magma toward the surface are rare. A question mark remains on the fact that this lack of well-documented upward an monotonic earthquake migration contemporary to magma ascent prior to an eruption could simply be an artefact due to a poor station coverage on many of the world's active volcanoes [Battaglia et al., 2005]. Available observations suggest however that, while vertical hypocenter migrations are uncommon, horizontal migrations appear to be more frequent (e.g. the 1978 Krafla intrusion [*Einarsson and Brandsdottir*, 1980], the 2000 Izu Islands magma migration [e.g. *Toda et al.*, 2002]).

From scale-invariance explorations [*Grasso and Bachelery*, 1995] and theoretical considerations [*Rubin and Gillard*, 1998], the distribution of recorded dyke-induced earthquakes is suggested to map the distribution of rock mass sites that are near to failure, and does not necessarily reflect the extent of the dyke. To note that only in the case of an homogeneous medium the maximum deformation occurs at the dyke head, where we therefore expect most of the seismicity to occur [*Lister*, 1990a; *Pinel and Jaupart*, 2004]. Besides,

earthquakes generated from the tensile propagation of the dyke tip are likely to be too small in magnitude [*Rubin*, 1995; *Rubin et al.*, 1998] and too high in frequency [*Cornet*, 1992] to be detected by standard seismic network that operate at volcano surface. The shear-type of the generally recorded seismicity accompanying magma movement, moreover, is not compatible with the signal associated to a dynamic propagation of the dyke tip (i.e. a tensile fracture) [*Cornet*, 1992].

Observations of Volcano-Tectonic (VT) seismicity during dyke propagation on basaltic volcanoes show a constant seismicity rate over time [*Traversa and Grasso*, 2009]. This characteristic pattern for the seismic signature of dyke propagation demonstrates to be reproducible on different volcanoes: Piton de la Fournaise (PdlF): 7 dyke intrusions in the period 1988-1992; Etna: 2002 dyke intrusion; and Miyakejima (MI): 2000 dyke intrusion.

For the Piton de la Fournaise dyke intrusions, *Traversa and Grasso* [2009] report diffuse VT seismicity within the shallow edifice. On these bases, *Traversa and Grasso* [2009] argue for the seismicity generated during dyke injection to be a generic response of the volcanic edifice to the intrusion instead of an accurate mapping of the dyke tip propagation.

Toda et al. [2002] show that the change in seismicity rate generated by the 2000 dyke intrusion at Izu Islands (Japan) scales with the change in stressing rate induced by the propagation and opening of the dyke. This result demonstrates that the stressing rate governs the seismicity. It moreover

supports the hypothesis of magma flow rate scaling with the seismicity rate [*Pedersen et al.*, 2007].

All these argue for the stationary seismicity rate accompanying the dyke propagation to be the response of the brittle lithosphere to a constant volumetric deformation rate (i.e. a constant influx of magma over time) induced by the intrusion [e.g. *Traversa and Grasso*, 2009].

Following *Traversa and Grasso* [2009] observations, the aim of this paper is therefore primarily (i) to analyze how a constant flow rate of magma injected into the dyke from the reservoir is consistent with the dynamics of a fluid-driven fracture propagating under realistic conditions for the magma chamber overpressure, and (ii) to evaluate the implications for the volcano dynamics. This is achieved by considering a two-phase dyke propagation model involving an initial vertical propagation phase followed by a horizontal migration phase.

Such two-phase propagation style for dyke propagating from a magma source at shallow depth to the surface, is commonly observed on basaltic volcanoes worldwide, e.g. Mt. Etna (southern Italy) [e.g. *Aloisi et al.*, 2006]; Miyakejima (southern Japan) [e.g. *Nishimura et al.*, 2001]; and in particular on Piton de la Fournaise [e.g. *Toutain et al.*, 1992; *Bachélery*, 1999; *Peltier et al.*, 2005, 2007].

For the vertical rise of a buoyant fluid-filled crack from a shallow storage system towards the surface, we consider two boundary conditions at the dyke inlet, constant and variable reservoir overpressure. In the latter case

the overpressure variation is controlled by the withdrawal of magma from the chamber induced by the dyke growth. Subsequently, the effect of a lithological discontinuity at depth is introduced by reducing the buoyancy of the fluid in the upper layer. This density step induces a slow down of the rising magma and favours melt accumulation and subsequent lateral dyke propagation.

We apply the two-phase dyke propagation model to the magmatic intrusion that fed the August 2003 Piton de la Fournaise (PdlF) eruption. The stationary rate of VT earthquakes accompanying the August 2003 PdlF dyke intrusion supports the result found by *Traversa and Grasso* [2009] in the 1992-1996 period. Accordingly we expect stationary flux of magma to feed the propagating dyke. Besides, the number of works devoted to its study make it one of the best studied intrusive episodes observed on PdlF volcano in the last years.

This application allows us to derive possible generic implications on the mechanisms driving magma movements on basaltic volcanoes. This so-called "proximal" eruption (according to *Peltier et al.* [2008] classification) is a good example to validate our model, first as being accompanied by a stationary seismicity rate over time, and second as being constituted of a vertical- and lateral-phase dyke propagation, which is the generally accepted feature describing flank eruptions at PdlF volcano [e.g. *Toutain et al.*, 1992; *Bachélery et al.*, 1998; *Bachélery*, 1999; *Peltier et al.*, 2005, 2007].

2. Models of dyke propagation

2.1. Vertical dyke propagation

In this section we focus on the vertical propagation of a buoyant fluid-filled crack, from a shallow storage system towards the surface (see figure 1). The crack is fed from a magma reservoir whose overpressure ΔP_c is either constant over time, or evolves as a consequence of the withdrawal of magma from the reservoir. In particular, the aim of this section, is to individuate whether and under which conditions, a magma reservoir is able to feed a propagating dyke with constant flux of magma input from the reservoir.

2.1.1. Model description

For simplicity we consider a two-layer elastic half-space, characterized by Poisson ratio ν and shear modululs G and subject to a lithostatic stress field. The magma-filled fracture originates from the roof of a magma reservoir located at depth H, which is taken as the reference level. The z-axis is oriented positively upwards, with $z = 0$ at the reference level, where magma (of density ρ_m) has developed the overpressure ΔP_c with respect to the surroundings. A lithological discontinuity is located at depth H_b, such that the rock density as a function of depth is given by (see figure 1)

$$\begin{aligned} \rho_r(z) &= \rho_{rl} \text{ for } z < H - H_b \text{ (lower layer)}, \\ \rho_r(z) &= \rho_{ru} \text{ for } z > H - H_b \text{ (upper layer)}. \end{aligned} \tag{1}$$

As demonstrated by previous authors [e.g. *Lister*, 1990a, b; *Lister and Kerr*, 1991], once the dyke length is large enough, the influence of the though-

ness of rocks on dyke propagation can be neglected. The fluid-filled crack propagation is in fact dominated by fluid dynamics, except during the early nucleation of the crack, [*Lister*, 1990a]. On these bases, we neglect the strength of the surrounding rocks in the force balance, and hence do not treat stress singularity at the tip. We focus instead on the interplay between buoyancy, viscous head loss and elastic stresses. By considering also flow-induced stresses, the stress induced by the dyke opening is given by [*Pinel and Jaupart*, 2000]:

$$\sigma_o(z) = \Delta P_c + \sigma_b(z) + p_v, \tag{2}$$

where p_v is the viscous head loss and $\sigma_b(z)$ is the magma overpressure due to buoyancy. $\sigma_b(z)$ is given by:

$$\sigma_b(z) = \int_0^z (\rho_r(z') - \rho_m) g dz', \tag{3}$$

Following *Pinel and Jaupart* [2000] and *Maaløe* [1998], we fix the dyke breadth a and we assume that the dyke adopts an elliptical cross section with semi-axes a and b characterized by $b(z,t) \ll a$, see figure 1. In this case, the dyke-induced stress is given by [*Muskhelishvili*, 1963]

$$\sigma_o(z,t) \approx \frac{G}{1-\nu}\frac{b(z,t)}{a}, \tag{4}$$

193 Magma is considered as Newtonian, viscous and incompressible. Flow
194 proceeds in a laminar regime. According to *Pinel and Jaupart* [2000], we
195 obtain the following equation for the case of null lateral stress variation:

$$\frac{\partial b(z,t)}{\partial t} = -\frac{1}{4\mu}\frac{\partial}{\partial z}\left(\frac{\partial \sigma_b}{\partial z} b^3\right) + \frac{G}{16\mu a(1-\nu)}\frac{\partial^2 b^4}{\partial z^2} \tag{5}$$

196 where μ is magma viscosity.

197 We scale the pressures by the initial overpressure within the magma reser-
198 voir, $\Delta P_c(t=0) = \Delta P_0$, and the front height z_f by the reservoir depth H.
199 Scales for time, flux and fracture width for the vertical propagation are the
200 following

$$[t] = \frac{16\mu H^2 G^2}{\Delta P_0^3 a^2 (1-\nu)^2}, \tag{6}$$

$$[Q] = \frac{(1-\nu)^3 \Delta P_0^4 a^4}{16 G^3 \mu H}, \tag{7}$$

$$[b] = \frac{\Delta P_0 a (1-\nu)}{G}. \tag{8}$$

201 These are the reference quantities in the computation, i.e. $[t]$ is the time-
202 scale for opening the crack over a length H with a uniform overpressure ΔP_0.
203 Length-scale $[b]$ is the fracture width originated by an overpressure ΔP_0. The
204 scale for the dyke propagation velocity is then given by: $[v] = H/[t]$. The
205 initiation of the fracture on the reservoir walls is imposed a priori with an
206 elliptical profile. This affects the fracture growth only for a duration needed
207 for an initial adjustment stage [*Ida*, 1999]. We can define three dimensionless

numbers. The dimensionless number R_{1l} characterizes the magnitude of the buoyancy force scaled to the initial overpressure, as follows

$$R_{1l} = \frac{(\rho_m - \rho_{rl})g\,H}{\Delta P_0} \tag{9}$$

Dimensionless numbers R_{1u} and R_2 characterize the lithological discontinuity, as follows:

$$R_{1u} = \frac{(\rho_m - \rho_{ru})g\,H}{\Delta P_0} \tag{10}$$

$$R_2 = \frac{H_b}{H} \tag{11}$$

We have therefore the following dimensionless problem to solve

$$\frac{\partial b\,(z,t)}{\partial t} \;=\; -4\frac{\partial}{\partial z}\left(\frac{\partial \sigma_b}{\partial z}b^3\right) + \frac{\partial^2 b^4}{\partial z^2}, \tag{12}$$

$$b_{(z=0,\,t)} \;=\; \Delta P_c(t); \tag{13}$$

When there is no lithological discontinuity, $R_{1l} = R_{1u} = R_1$, and equation 12 reduces to:

$$\frac{\partial b\,(z,t)}{\partial t} = 4R_1\frac{\partial b^3}{\partial z} + \frac{\partial^2 b^4}{\partial z^2}, \tag{14}$$

This is solved numerically using a semi-implicit finite difference scheme with Dirichlet boundary conditions.

In this framework, equation 12 allows to follow the dynamics of dyke propagation on its way towards the surface. We checked that mass conservation

was satisfied on the scale of the whole dyke, which requires the instantaneous volume change to be equal to the basal flux, both values being issued from the numerical computation. The dimensions of the fracture at its base (i.e. the imposed a value and the calculated $b(0,t)$, which depends on the overpressure at the dyke inlet) determine the volume of magma intruding into the fissure per time unit. The velocity of the dyke propagating towards the surface is given by dz_f/dt, where z_f is the fracture front height (see figure 1).

When magma is injected from the reservoir into the dyke, it induces a decrease of the magma reservoir volume ΔV_c, which might in turn induce a decrease of the reservoir overpressure ΔP_c as well. Considering the elastic deformation induced by a point source (i.e. the magma reservoir) embedded in an infinite medium, the evolution of the reservoir overpressure follows the equation [V. Pinel and C. Jaupart, 2009, personal communication]:

$$d\,\Delta P_c(t) = \frac{dV_c(t)}{V_c(t)} \frac{4KG}{4G+3K} \tag{15}$$

where K is the magma bulk modulus. The volume variation in the magma reservoir can be related to the volume of magma injected into the dyke by

$$dV_c(t) = -Q(t)dt, \tag{16}$$

with Q the flux of magma entering the dyke. When magma is fully compressible, $K = 0$ and the magma reservoir overpressure remains constant trough time. For incompressible magma, $K \to \infty$ and equation 15 becomes

$$d\Delta P_c(t) = \frac{dV_c(t)}{V_c(t)} \frac{4G}{3} \tag{17}$$

238 To fully describe the evolution of the reservoir pressure, we introduce two
239 new dimensionless numbers:

$$R_3 = \frac{\Delta P_0 \, a^2 \, (1-\nu) \, H}{G \, V_c}, \tag{18}$$

240 which is the inverse dimensioneless reservoir volume, and

$$R_4 = \frac{4KG}{\Delta P_0 \, (4G + 3K)}. \tag{19}$$

241 which relates the overpressure variation in the reservoir to the initial over-
242 pressure value.

243 2.1.2. Results

244 We study the propagation of a vertical dyke from a shallow reservoir, ac-
245 cording to the geometry illustrated in figure 1. We investigate under which
246 conditions the magma flux injected into the dyke remains constant during
247 dyke growth. Using the dimensionless numbers above described, we discuss
248 the role played by each parameter in determining the regime of magma flux
249 carried by the rising dyke. We solve the problem for three different configu-
250 rations, described here below.

251 (i) Dyke rising from a constant overpressure magma reservoir in a homoge-
252 neous medium,

253 (ii) Dyke rising from a variable overpressure magma reservoir in a homoge-

neous medium,

(iii) Dyke rising from a variable overpressure magma reservoir in a layered medium.

First we consider the case of a dyke rising from a constant overpressure magma reservoir ($\Delta P_c = \Delta P_0 = \text{const.}$) in a homogeneous medium (i.e. $\rho_{rl} = \rho_{ru}$, $R_{1l} = R_{1u} = R_1$). As shown in figure 2, after some numeric adjustment iterations (whose number decreases with R_1 value), the flux of magma in the growing dyke evolves similarly to the propagation velocity (figure 2, A and B). This is related to the fact that, in this case, the dyke growth depends on tip propagation. Since fracture half-breadth a is assumed constant a priori and the medium is homogeneous, the dyke only grows along the propagation direction (figure 2, C). In this first case, the only dimensionless number affecting the regime of magma flux over time is R_1. We consider as negligible a flux variation less than 5% between dimensionless dyke heights $z_f = 0.3$ and $z_f = 0.9$. The choice of the first limit is imposed by discarding initial numerical adjustment iterations. As shown in figure 3 (black open squares), the magma flux withdrawn from the reservoir remains constant during dyke rising for $R_1 \leq -3.55$. In this constant overpressure case, and for a given reservoir depth, the only parameter determining the regime of the magma flux carried by the growing dyke is the ratio between the buoyancy force and the magma overpressure at the dyke inlet.

Second we consider the same case as above, but with the reservoir overpressure varying as magma is withdrawn. Through the dimensionless numbers

R_3 and R_4, we explore the role of the magma chamber volume V_c and of the magma bulk modulus K, which relates changes in reservoir volume with changes in pressure, on the regime of magma flux withdrawn from the reservoir. As illustrated in figure 3 (plain symbols), the smaller the dimensionless number R_3, the more the flux tends to remain constant during dyke propagation and viceversa. It means that the larger the chamber volume with respect to the dyke scale volume, the more negligible a withdrawal of magma is in terms of variations in magma flow rate and reservoir overpressure during dyke rising. In the same way, the smaller the dimensionless number R_4, the smaller the magma flux variation obtained during dyke rising and viceversa. This implies that the more the magma tends to be incompressible, i.e. $K \to \infty$, the more the flow of magma injected into the dyke varies over time as the dyke propagates. As shown in figure 3 legend, this scenario corresponds to larger variations in the reservoir overpressure ($\Delta P_c\, variation$) face to the withdrawal of magma from the reservoir. Conversely, more compressible magmas, i.e. $K \to 0$, allow for smaller variations in the magma flow rate over time, which correspond to smaller overpressure variations accompanying magma withdrawn from the reservoir. However, only small overpressure variations ($\Delta P_c\, variation$ less than $\sim 2\%$) in the magma reservoir allow for the magma flow rate to remain constant during dyke propagation.

As a third case we consider a lithological discontinuity within the volcanic edifice. This discontinuity is intended in terms of rock densities, which are chosen such that magma has intermediate density between the lower and

upper rock layers ($\rho_{rl} < \rho_m < \rho_{ru}$). This allows for considering a twofold effect: on one hand the higher fracturation of the solid medium close to the surface, which implies a lower density of the shallow layer and, on the other hand, the fact that magma degasses while rising, becoming more and more dense as approaching the surface. The effect of this density step is to slow down the rise of magma, creating favorable conditions for magma accumulation at the discontinuity depth H_b.

Figure 4 illustrates the variation of the dimensionless magma flux, propagation velocity, and dyke shape during dyke propagation from an overpressured magma chamber, in a two-layer medium. After an initial numeric adjustment transient, the magma flux remains constant over time, being blind to the lithological discontinuity (figure 4A). The dyke volume continues therefore to regularly grow as dyke rises. On the other hand, the dyke propagation velocity, computed as dz_f/dt, significantly decreases when the dyke reaches the depth of the density step (figure 4B), as also shown by *Taisne and Jaupart* [in press, 2009].

Reminding that the seismic response of a volcanic edifice to dyke propagation is reported to be stationary over time [*Traversa and Grasso*, 2009], this result supports the hypothesis of scaling between seismicity rate accompanying the dyke intrusion and the volumetric flux of magma entering the dyke. On the other hand, it excludes the possibility of a direct scaling between the seismicity rate and the dyke propagation velocity. The density step does not affect the shape of the fracture at the dyke inlet (figure 4C). In our model,

for a given magma viscosity, the magma flux supply only depends on the shape of the crack at the junction with the reservoir roof. It can therefore remain constant over time as dyke grows.

While dyke half-breadth a is assumed to be constant over time, the dimensionless numbers R_{1rl}, R_{1ru} and R_2 play a role in determining the width of the dyke at the inlet, and therefore the regime of magma flux carried by the propagating dyke. The parameter R_{1rl} has been discussed above, while figure 5 shows the effect of R_{1ru} and R_2 dimensionless numbers on the regime of magma flow over time. In analogy with the previous discussion, we consider as negligible a variation in the magma flux less than 5% between dimensionless front heights $z_f = 0.3$ and 0.9. Variation in magma flux during dyke rise are negligibile for $R_{1ru} < 1.5$ and for $R_2 < 0.5$. These imply that, in order for the flux of magma to remain constant over time, the densities of the magma and the upper layer should be quite close in value, and that the discontinuity should not be deeper than half the reservoir depth.

As shown in figure 13C, when magma buoyancy faints, due to a decrease in the surrounding rock density, an inflation starts to grow at the dyke head. Here elastic stresses may exceed the rock toughness and new fractures may initiate.

2.2. Lateral propagation at the Level of Neutral Buoyancy

Exhaustive description of the solution for dyke propagation at a lithological boundary fed by either, constant flux or constant volume of magma is given by *Lister* [1990b] and *Lister and Kerr* [1991]. They assume that

buoyancy forces do not depend on horizontal distance. The effects of lateral variations of the stress field induced by a volcanic edifice load on the lateral propagation are studied by *Pinel and Jaupart* [2004]. In this paper we consider an horizontal lithological boundary located within the volcanic edifice. We therefore adapt the solutions given by *Pinel and Jaupart* [2004] in order to take into account the variation of the external lithostatic pressure induced by the volcano slope along the propagation direction.

2.2.1. Model description

Figure 6 illustrates the geometry and main parameters used in this section. ρ_{ru} and ρ_{rl} are, respectively, the rock densities in the upper and lower layer. For this case, we define the origin of the vertical coordinate z at the discontinuity level, oriented positive upwards. The vertical extension of the dyke is called $2a(x)$. $z_u(x)$ and $z_l(x)$ stands for the positions of the upper and lower dyke tips respectively, such that we have:

$$2a(x) = z_u(x) - z_l(x) \tag{20}$$

We also define

$$m = \frac{z_u + z_l}{z_u - z_l} \tag{21}$$

We neglect the effects of the free surface [*Pinel and Jaupart*, 2004], so that the stress generated by the pressure difference between the interior and the exterior of the dyke, σ_o, is given by

$$\sigma_o(x,z) \;=\; (\rho_{ru} - \rho_m) g\, z - \sigma_l(x) + p, \quad \text{if } z > 0 \tag{22}$$

$$\sigma_o(x,z) \;=\; (\rho_{rl} - \rho_m) g\, z - \sigma_l(x) + p, \quad \text{if } z < 0, \tag{23}$$

where p is the internal magma pressure, which varies due to viscous friction, and σ_l is the lithostatic pressure at the lithological boundary, defined by:

$$\sigma_o(x) = \rho_{ru} g (H_b - \theta x), \tag{24}$$

with θ the volcano slope.

We consider that the lateral dyke length is larger than its height and we neglect vertical pressure gradients due to upward flow within the dyke [*Lister and Kerr*, 1991; *Pinel and Jaupart*, 2004]. In this case, the internal magma pressure p depends only on the lateral position x. As before, the condition for the crack to remain open is $\sigma_o > 0$.

We consider that the dyke propagates in damaged rocks, and therefore we set to zero the stress intensity factor at both dyke tips [*Mériaux et al.*, 1999]. Following *Pinel and Jaupart* [2004], this leads to

$$\arcsin m + m\sqrt{1-m^2} = \frac{\pi}{2} \frac{\rho_{rl} + \rho_{ru} - 2\rho_m}{\rho_{rl} - \rho_{ru}} \tag{25}$$

$$\sigma_o(x, z=0) = \frac{g}{\pi} (\rho_{rl} - \rho_{ru}) a(x) (1-m^2)^{3/2} \tag{26}$$

It means that for given values of densities ρ_{ru}, ρ_{rl} and ρ_m, once the overpressure at the lithological discontinuity is known at a given lateral distance

x, there is a unique solution for the half-height $a(x)$ and the tip locations $z_u(x)$ and $z_l(x)$. This solution can be subsequently used to calculate the dyke width $b(x,z)$ using the solution derived from *Pinel and Jaupart* [2004]. For $-1 < s < 1$, the half-width $b(s)$ is given by:

$$\begin{aligned} b(s,x) = & \ \tfrac{(1-\nu)\sigma_o(x,z=0)}{G}\sqrt{1-s^2} \\ & + \ \tfrac{a(x)(1-\nu)g(\rho_{rl}-\rho_{ru})}{G\pi} \quad [\sqrt{1-s^2}(-\frac{1}{2}\sqrt{1-m^2}-\frac{1}{2}s\arcsin m - m\arcsin m) \\ & \quad -\frac{1}{2}(s+m)^2\ln|\frac{1+sm+\sqrt{(1-s^2)(1-m^2)}}{s+m}| \\ & \quad +\frac{\rho_{ru}+\rho_{rl}-2\rho_m}{\rho_{rl}-\rho_{ru}}\sqrt{1-s^2}(\frac{1}{4}s\pi+\frac{1}{2}m\pi)] \end{aligned} \tag{27}$$

where s is defined by:

$$s = \frac{z}{a(x)} - m.$$

From equation 25, we can see that dyke extension in the upper medium is equal the extension in the lower medium ($m = 0$) just in case $\rho_{rl} - \rho_m = \rho_m - \rho_{ru}$. As there is no lateral variations of the stress field vertical gradient, m is a constant.

The dyke internal pressure σ_o, which keeps the dyke open, varies laterally because of both, the volcano flank slope and the viscous head losses due to horizontal magma flow. Magma is considered as Newtonian, viscous and incompressible. Flow proceedes in laminar regime.

Following *Pinel and Jaupart* [2004] analytical procedure, the dyke half-height $a(x,t)$, is the solution of the following equation

$$c_1\, g(\rho_{ru}-\rho_m)\frac{\partial a(x,t)^3}{\partial t} =$$

$$\frac{c_3(1-\nu)^2}{3\mu\, G^2}\frac{\partial}{\partial x}\left[a(x,t)^7 g^3(\rho_{ru}-\rho_m)^3\left(\frac{g(\rho_{rl}-\rho_{ru})}{\pi}(1-m)^{3/2}\frac{\partial a(x,t)}{\partial x}-\rho_{ru}g\theta\right)\right]. \quad (28)$$

where

$$c_n = \int_{-1}^{1} f(s)^n ds, \quad (29)$$

$$f(s) = \frac{Gb(s)}{g(1-\nu)(\rho_{ru}-\rho_m)a(x)}. \quad (30)$$

We scale the pressures by the lithostatic load of the rock mass above the density step,

$$[P] = \rho_{ru}\, g\, H_b. \quad (31)$$

the flux by the input flux of magma Q_{in} and all length dimensions by the depth of the lithostatic discontinuity H_b. The scale for the time refers to the opening of a fissure over a length H_b with a magma flux equal to Q_{in}, and is given by the following equation:

$$[t] = \left(\frac{\mu\ (1-\nu)\, H_b^9}{G\, Q_{in}^3}\right)^{1/4}, \quad (32)$$

As shown by *Pinel and Jaupart* [2004], two dimensionless numbers can be defined:

$$N_1 = \frac{3Q_{in}^{3/4}\mu^{3/4}G^{9/4}}{H_b^{9/4}(1-\nu)^{9/4}[P]^3} \quad (33)$$

$$N_2 = -\frac{2H_b^3(1-\nu)^3[P]^4}{3\mu Q_{in}G^3} \quad (34)$$

400 Equation 28 can be rewritten in the dimensionless form:

$$\frac{c_1}{c_3}N_1\frac{\rho_{ru}-\rho_m}{\rho_{ru}}\frac{\partial a^3}{\partial t} = -\theta\frac{(\rho_{ru}-\rho_m)^3}{\rho_{ru}^3}\frac{\partial a^7}{\partial x} + \frac{(1-m)^{3/2}(\rho_{ru}-\rho_m)^3(\rho_{rl}-\rho_{ru})}{8\pi\rho_{ru}^4}\frac{\partial^2 a^8}{\partial x^2} \quad (35)$$

401 The dimensionless flux is given by:

$$\frac{q}{Q_{in}} = N_2 c_3 a(x,t)^7\frac{(1-m)^{3/2}(\rho_{ru}-\rho_m)^3(\rho_{rl}-\rho_{ru})}{8\pi\rho_{ru}^4}[\frac{\partial a(x,t)}{\partial x} - \theta] \quad (36)$$

402 We solve numerically this equation with a semi-implicit finite difference
403 scheme with a Neumann boundary conditions at the source ($x = 0$).

404 **2.2.2. Results**

405 In this section we discuss the effect of the model parameters on the propa-
406 gation of a dyke at a lithological boundary, fed by a constant flux of magma.
407 As discussed in the previous section, the dyke propagation is affected by the
408 variation in the external lithostatic pressure induced by the volcanic slope
409 along the propagation direction, while vertical stress gradients do not vary
410 laterally.

411 *Lister* [1990b], discusses the case of a dyke fed by constant flux or constant
412 volume of magma, laterally propagating in a medium with no lateral stress
413 variations. In this case the breadth of the dyke ($2a(x)$ in figure 6) varies in
414 time all along its length, being however always largest at the origin ($2a(x =$
415 $0)$). *Pinel and Jaupart* [2004] consider the effect of the volcanic edifice load

on the propagation of a lateral dyke at depth. In this case, the breadth of the dyke varies at the head during lateral propagation, due to lateral variations of vertical stress gradients. For the present case, the lateral stress variations are only due to the flank slope of the edifice. Figure 7 shows that, with small flank slopes ($\theta \rightarrow 0$), the breadth of the dyke grows at the origin as the dyke propagates, reminding the case discussed by *Lister* [1990b]. With higher flank slopes, the half-breadth a tends to a constant value as the dyke laterally propagates. Such constant value does not depend on the propagation distance from the origin. In this sense, the effect of the volcano flank slope θ is such that it carries back to the previously discussed vertical propagation case, where the breadth $2a$ of the dyke was assumed to be constant during propagation.

3. Case study: The August 22 2003, Piton de la Fournaise eruption

3.1. Overview on PdlF storage and eruptive system

The Piton de la Fournaise (PdlF), Reunion Island, Indian Ocean, is a well-studied basaltic intraplate strato-volcano, with a supply of magma from hotspots in the mantle [see e.g. *Lénat and Bachèlery*, 1990; *Aki and Ferrazzini*, 2000; *Battaglia et al.*, 2005; *Peltier et al.*, 2005, among others]. There are five conceptual models describing the shallow storage system at PdlF volcano. First, *Lénat and Bachèlery* [1990] propose a model of summit reservoir composed by many small independent shallow magma pockets, located above sea level at a depth of about 0.5-1.5 km beneath Dolomieu crater. This model is supported by the cellular automaton model of *Lahaie and Grasso* [1998]

437 during the 1920-1992 period, which considers basaltic volcanoes as complex
438 network of interacting entities at a critical state. A 1-10 x 10^6 m^3 volume
439 has been estimated for such magma batches through spatial extent of seis-
440 micity [*Sapin et al.*, 1996]. This range spans the volumes of lava emitted
441 by the eruptions occurred at PdlF in the period 1972-1992 [*Sapin et al.*,
442 1996; *Peltier et al.*, 2009], while about 32% of eruptions occurred since 1998
443 emitted lava volumes larger than 10 x 10^6 m^3 [*Peltier et al.*, 2009].

444 Second *Sapin et al.* [1996], on crystallization arguments point out, however,
445 that in order to produce eruptions with lava volumes of order 1-10 x 10^6 m^3,
446 the volume of magma in the chamber needs to be larger than the emitted
447 volume. They therefore suggest, as a better candidate for the Piton de
448 la Fournaise magma reservoir, the low seismic-velocity zone identified by
449 *Nercessian et al.* [1996] at about sea level. This aseismic zone is located just
450 below the depth at which pre-eruptive seismic swarms are generally located,
451 and extends at depths of 1.5-2 km below sea level. It implies a second magma
452 chamber model volume of 1.7-4.1 km^3.

453 Third, *Albarède* [1993], by applying Fourier analysis of the Ce/Yb fluctua-
454 tions in the Piton de la Fournaise lavas over the 1931-1986 period, estimates
455 a magma residence time in the reservoir between 10 and 30 years. This re-
456 sult, combined with magma production rates, lead the author to conclude
457 that the maximum size of the PdlF magma chamber may hardly exceed 1
458 km^3.

Fourth *Sigmarsson et al.* [2005] uses ^{238}U-series desequilibria of basalts erupted at PdlF during the period 1960-1998 to estimate magma residence time and to infer a volume of 0.35 km^3 for the Piton de la Fournaise shallow magma reservoir.

Five, *Peltier et al.* [2007, 2008], on tilt, extensometer and GPS data basis, describe the PdlF eruptions since 2003, as fed from a common magma chamber located at a depth of 2250-2350 m beneath the summit and with a radius of $\sim$ 500 m. This corresponds to a reservoir volume of about 0.5 km^3. The eventuality of deeper storage systems has been discussed by *Aki and Ferrazzini* [2000], *Battaglia et al.* [2005], *Prôno et al.* [2009] and *Peltier et al.* [2009]. Hence, the presence, location and size of reservoirs below Piton de la Fournaise still remain an open question.

As discussed in previous studies [e.g. *Toutain et al.*, 1992; *Bachélery et al.*, 1998; *Peltier et al.*, 2005], flank eruptions at Piton de la Fournaise generally consist of two phases: an initial vertical rise of magma followed by a near-surface lateral migration towards the eruption site.

For the 2000-2003 period, *Peltier et al.* [2005] observe a correlation between the duration of the lateral propagation stage and the distance of the eruptive vents from the summit. Since the seismic crisis onset coincides with the beginning of the first propagation phase [e.g. *Peltier et al.*, 2005, 2007; *Aki and Ferrazzini*, 2000], *Peltier et al.* [2005] calculate a mean vertical speed of about 2 m s^{-1}, while lateral migration velocities range between 0.2 and 0.8 m s^{-1}. This results are similar to those reported by *Toutain et al.* [1992]

for the April 1990 PdlF eruption (i.e. 2.3 m s^{-1} for the verical propagation and 0.21 m s^{-1} for the lateral migration) and *Bachélery et al.* [1998] for the eruptions taking place during the first sixteen years of the PdlF Observatory (1980-1996).

In this paper we focus on the August 2003 dyke intrusion, which has been extensively studied through extensometer, tiltmeter, GPS and INSAR data by *Peltier et al.* [2005, 2007], *Froger et al.* [2004] and *Tinard* [2007]. The dyke intrusion is accompanied by a seismic crisis of around 400 volcano-Tectonic (VT) events within 152 min (figure 8).

Seismic data illustrated in figure 8 confirm for the August 2003 case the seismic rate stationarity observed by *Traversa and Grasso* [2009] for the PdlF intrusions in the 1988-1992 period.

3.2. Relationships between magma flux regime and initial conditions for magma reservoir

Following the results obtained in section 2.1.2 for the vertical propagation stage, and referring to the parameters listed in table 1, we can calculate an upper bound for the reservoir initial overpressure and a lower bound for the magma reservoir volume values, such that the reservoir is able to sustain a constant influx magmatic intrusion.

The upper bound for the reservoir overpressure able to sustain a constant magma flux injection, can be computed by referring to the vertical propagation stage within a homogeneous medium (i.e. we neglect the effect of the upper layer, dimensionless number $R_2 = 0$). We choose a large magma reser-

503 voir volume with fully compressibile magma (i.e. $R_3 \to 0$, $R_4 \to 0$). The
504 upper limit for the initial reservoir overpressure is given by the dimensionless
505 number R_1 corresponding to less than 5% variation in the magma flux during
506 dyke growth (see figure 3, black empty squares). This is: $R_1 < -3.55$.

507 For parameters listed in table 1, this implies an initial reservoir overpres-
508 sure $\Delta P_0 < 2.2$ MPa. Such upper limit is compatible with the average
509 overpressure a the dyke inlet estimated for the August 2003 PdlF dyke in-
510 trusion, i.e. 1.7 MPa using InSAR data [*Tinard*, 2007] and at 1.1 MPa using
511 GPS and tiltmeter data [*Peltier et al.*, 2007]. Dyke inlet overpressure values
512 computed using GPS data for PdlF eruptions between 2004 and 2006 also
513 are in the range 1.1 - 2.2 MPa [*Peltier et al.*, 2008].

514 Note that this value is one order smaller than commonly observed rock
515 resistances. It may be characteristic of PdlF volcano, wich endured 25 erup-
516 tions in the period 1998-2007 [*Peltier et al.*, 2009].

517 As regarding to the generic lower bound for the magma reservoir volume
518 able to sustain a constant magma influx intrusion, we already discussed in
519 section 2.1.2 the influence of the dimensionless numbers R_3 and R_4 on the flux
520 regime of the propagating dyke. As shown in figure 9 for the vertical dyke
521 propagation within a homogeneous medium case, a magma compressibility
522 K of about 1 GPa implies that the minimum reservoir volume required for
523 the flux of magma to remain constant over time is $> 1\,\mathrm{km}^3$. The volume
524 of magma mobilized by the lateral injection has the effect of increasing the
525 minimum size of the magma reservoir required in order to keep the flux

constant over the two-phase dyke propagation. In addition, the smaller the magma chamber volume, the smaller the R_1 value necessary to keep the magma flux constant over time. For given reservoir depth, magma and rock densities, this implies smaller initial overpressures sustaining a constant influx of magma over time will be.

3.3. Relationship between magma volumes and reservoir overpressure conditions

Traversa and Grasso [2009] assimilate the intrusion process on basaltic volcanoes to a strain-driven, variable-loading process, reminiscent of secondary brittle creep. In such a strain-driven process, the loading is free to vary over time. It means that the overpressure at the dyke inlet is free to vary over time.

Most of PdlF eruptions occurring in the last decades, however, are flank eruptions, with eruptive vents located close or within the central cone, [*Peltier et al.*, 2005, 2007, 2008]. According to the model proposed by *Peltier et al.* [2008] for the magma accumulations and transfers at PdlF since 2000, there is a hierarchy between the so-called 'distal' eruptions (occurring far from the summit cone), which release the reservoir overpressure, and 'proximal' or 'summit' eruptions (occurring close to or within the summit cone), which have negligible effect on the reservoir overpressure state. In this sense, we therefore expect most of PdlF recent eruptions to be accompanied by small variations of the magma reservoir overpressure.

For the August 2003 PdlF eruption, the total amount of magma withdrawn from the reservoir (i.e. the volume of lava emitted plus the volume of the dyke that keeps stuck at depth) has been estimated by *Peltier et al.* [2007] and *Tinard* [2007] at 7.2 and 7.8 x 10^6 m^3, respectively.

The model of small independent magma pockets proposed by *Lénat and Bachèlery* [1990] implies a substantial emptying of the lens feeding each individual eruption. This is consistent with large overpressure variations accompanying the dyke intrusion. On the other hand, for the other four conceptual models proposed for the PdlF reservoir system, i.e. reservoir volumes of 1.7-4.1 km^3 [*Nercessian et al.*, 1996; *Sapin et al.*, 1996], 0.1-0.3 km^3 [*Albarède*, 1993], 0.35 km^3 [*Sigmarsson et al.*, 2005] and 0.5 km^3 [*Peltier et al.*, 2007, 2008], the magma volume withdrawn from the chamber during the August 2003 eruption represents between $\sim$ 0.2% and $\sim$ 2.5% of the reservoir volume. These values argue for very small overpressure variations accompanying the dyke intrusion.

In order to test which of these configurations (i.e. large or small overpressure variations) applies to the PdlF case, we calculate the minimum reservoir size that would be required for the overpressure to vary of a defined small percentage during dyke injection. By integrating equation 15 we obtain:

$$V_c = \frac{\Delta V_c}{exp\left(\Delta P_{c\,var}\left(\frac{4G+3K}{4GK}\right)\right) - 1}. \tag{37}$$

where ΔV_c is the variation in reservoir volume, $\Delta P_{c\,var}$ is the variation in reservoir overpressure induced by the dyke intrusion, G is the rock shear modulus, and K is the magma bulk modulus.

We assume that the volume variation induced in the magma reservoir from the August 2003 dyke growth corresponds to the estimations of the dyke volume, i.e. $\Delta V_c = 1 - 1.6$ x $10^6 \mathrm{m}^3$ [*Peltier et al.*, 2007; *Tinard*, 2007]. This is related to the fact that observations of seismicity rate during dyke injection [*Traversa and Grasso*, 2009] do not give any information about the flux evolution after the eruptive activity begins. We thus limit the validity of the constant influx model only to the dyke injection, allowing that possible larger pressure and flux variations could occur during lava flow at surface. The estimated volume of lava erupted during the August 2003 eruption is 6.2 x $10^6 \mathrm{m}^3$ [*Peltier et al.*, 2007]. The total volume of magma withdrawn from the chamber is therefore as large as 7.2-7.8 x 10^6 m^3.

We take as the initial reservoir overpressure the upper bound we calculated previously, i.e. $\Delta P_0 = 2.2$ MPa and we compute the reservoir volume required for the magma overpressure variation $\Delta P_c\, variation$ to be the 5% of the initial reservoir overpressure, i.e. ~ 0.085 MPa. Equation 37 gives $V_c = 5 - 8$ km^3 as the corrisponding reservoir size.

When applying our model for vertical dyke propagation, computations of overpressure variations induced in a realistic reservoir ($V_c = 0.5 - 5$ km^3 [*Nercessian et al.*, 1996; *Sapin et al.*, 1996; *Peltier et al.*, 2007, 2008]) by a vertical dyke fed at constant flux, are showed in figure 3 legend. These

variations are $< 6\%$, for reservoir volumes between 0.5 and 5 km^3 and magma compressibility between 1 and 10 GPa.

3.4. Relationships between constant magma influx and dyke injection dynamics

In this section we derive the implications of the two-phase model on dyke injection dynamics and we test the model for the dyke intrusion that fed the August 2003, Piton de la Fournaise eruption.

The August 2003 PdlF eruption involves three eruptive fissures, the first within the summit zone (at 17h20 UTM), the second on the northern flank, at 2475 m asl (at 18h10 UTM), and the third lower on the northern flank, at about 2150 m asl (at 19h30 UTM) [Staudacher, OVPF report]. The eruptive activity of the first two fissures was negligible compared to the last one (the former stopped at the end of the first day of the eruption, while only the third fissure remained active throughout the eruption) [*Peltier et al.*, 2007, and Staudacher OVPF report]. As modeled by deformation data, the intrusion preceding this PdlF eruption includes a $\sim$20 minutes duration (from 14h55 to 15h15 UTM) vertical dyke propagation followed by a $\sim$125 minutes (from 15h15 to 17h20 UTM) lateral injection toward the north [*Peltier et al.*, 2007]. Although the 17h20 UTM time corresponds to the opening of the first summit fracture [Staudacher OVPF report], tilt data clearly indicate that the lateral dyke has already fully propagated to the flank eruption site by this time. Indeed, no further evolution of the deformation is observed after 17h20 UTM [*Peltier et al.*, 2007].

By inverting deformation data, *Peltier et al.* [2007] estimate the origin of the August 2003 dyke at 400 ±100 meters asl, and the origin point of the lateral dyke at 1500 ±350 m asl. The lateral dyke travels 2.4 ±0.1 km before breaching the surface [*Peltier et al.*, 2007]. On deformation data basis, *Peltier et al.* [2007] estimate an average velocity of 1.3 $\mathrm{m\,s^{-1}}$ for the vertical rising stage, and of 0.2 - 0.6 $\mathrm{m\,s^{-1}}$ for the lateral injection phase. The uncertainties related to vertical and horizontal propagation velocities, obtained from deforamtion data inversion, are 0.26 $\mathrm{m\,s^{-1}}$ and 0.13 $\mathrm{m\,s^{-1}}$, respectively [uncertainties from A. Peltier 2009, personal communication].

In the following we calibrate the input parameters for the two-stage dyke propagation model. First we derive the relationships among the parameters at stake for the two steps. Second we obtain calibrations of the same parameters by using indepedent estimates of dyke propagation velocities in the two phases.

We consider a dyke rising vertically within a homogeneous medium (i.e. $R_2 = 0$), from a large magma reservoir with fully compressible magma (i.e. $R_3 \to 0$, $R_4 \to 0$). Reservoir depth H, magma and rock densities ρ_m, ρ_r are listed in table 1. In this case, the flux of magma injected into the dyke only depends on the initial overpressure at the dyke inlet and is inversely proportional to the magma viscosity,as shown in figure 10:

$$Q \propto \frac{1}{\mu}, \tag{38}$$

When we fix the vertical velocity and we let the dyke half-breadth a free to vary, however, we can write:

$$Q = A\,\mu, \tag{39}$$

where

$$A = \frac{v_v^2\, Q^*\, 16 H\, G}{v_v^{*2}\, \Delta P_0^2\, (1-\nu)} \tag{40}$$

v_v is the vertical propagation velocity, Q^* is the dimensionless flux of magma entering into the dyke (i.e. $Q/[Q]$) and v_v^* is the dimensionless vertical propagation velocity (i.e. $v_v/[v]$). The vertical propagation velocity, in turn, is given by

$$v_v = C\frac{a^2}{\mu}. \tag{41}$$

where

$$C = \frac{v_v^*(1-\nu)^2\, \Delta P_0^3}{16\, H\, G^2}. \tag{42}$$

For a given dimensionless number R_1, the dimensionless flux and velocity (i.e. Q^* and v_v^*) are fixed. Then, for given values of vertical propagation velocity, depth of the reservoir, and initial magma overpressure, we obtain the A value.

641 We take $R_1 = -3.55$ (i.e. the upper limit for a 5% flux variation in
642 the constant reservoir overpressure, homogeneous medium case as shown in
643 figure 3) and the parameters listed in table 1.

644 The lateral propagation velocity depends on the magma viscosity and on
645 the amount of magma injected into the dyke in the unit time. We then in-
646 ject different magma flux and viscosity pairs into the lateral dyke. Figure 11
647 shows how the magma flux injected in the dyke is related to the lateral prop-
648 agation velocity. In particular, a dyke lateral propagation velocity between
649 0.2 and 0.6 m s^{-1} (shadow box in figure 11), requires the magma flow rate
650 injected into the laterally migrating dyke to be less than about 60 $m^3 s^{-1}$.
651 Through equation 39 this implies a magma viscosity $\mu = 14\,\mathrm{Pa\,s}$. This allows
652 to constrain the value of the vertical dyke half-breadth $a = 100$ m (equation
653 41).

654 The value we estimate for viscosity is in good agreement with the values
655 found by *Villeneuve et al.* [2008] for remolten basalts from the 1998 lava
656 flow of the Piton Kapor, on the northern part of Dolomieu crater. Viscosity
657 measurement experiments conducted at constant stress indicate (i) liquidus
658 temperature of the 1998 sample at about 1200°C and (ii) viscosities between
659 49 and 5 Pa s measured at temperatures between 1195°C (glass transition)
660 and 1386°C (superliquidus), respectively.

661 For the case of a dyke propagating within a stratified medium from a
662 finite size, compressible magma chamber, more parameters play a role in
663 characterizing the dyke propagation, i.e. magma bulk modulus K, magma

chamber volume V_c, rock densities in the upper ρ_u and lower ρ_l layers and the depth of the lithological discontinuity H_b. We refer to the geometry illustrated in figure 12, and we use the parameters listed in table 2 in the calculations. Table 3 compares results issued from the computation with independent parameter estimates.

From the computation we obtain a dyke which rises vertically at an average velocity of $\sim$1.2 m s^{-1} up to the lithological discontinuity. Figure 13 shows the effect of the density barrier on the propagation of the vertical dyke. It quantifies injected magma flux and volume and dyke vertical propagation velocity over time (figure 13A, B, C). The shape of the vertical dyke for different propagation steps is illustrated in figure 13, D. The flow of magma injected into the vertical dyke over time is $\sim$35 m^3 s^{-1}, through a fracture of width $b \sim 30$ cm, which matches with the value found by *Peltier et al.* [2007], *Froger et al.* [2004] and field observations [*Peltier et al.*, 2007].

The dyke extends above the discontinuity, but its upward propagation is set back by the negative buoyancy [*Pinel and Jaupart*, 2004]. At the density step depth, magma overpressure grows as the dyke head inflates. It may eventually exceed rock thoughness and a new fracture may propagate laterally away. Here we set up a lateral dyke, which propagates towards the northern flank. We assume all the magma flux rising through the vertical dyke is injected into the lateral one. The slope of the edifice and the lack of lateral variation in stress gradients, allow for the dyke half-breath a to be constant during the lateral propagation (see figure 7).

687 The computed lateral dyke breadth $2a$ is $\sim$950 m. The upper bound of the
688 fracture breaches the surface at a height of about 2000 m asl after 2.3 km
689 lateral propagation, in agreement with field observations of eruptive fracture
690 location [*Peltier et al.*, 2007; *Tinard*, 2007]. The average propagation velocity
691 we compute for the lateral dyke is ~ 0.48 m s^{-1}, in agreement with the upper
692 limit value estimated by *Peltier et al.* [2007] by deformation data inversion
693 (0.2 to 0.6 m s^{-1}).

694 We remind that the flux of magma injected in the vertical and lateral dykes
695 is related to the respective initial dyke breadth. From the computation we
696 get lateral dyke breath ($a = 476$ m) about five times the vertical dyke one
697 ($a = 100$ m). This is related to the fact that horizontal velocity is much
698 lower than the vertical, which has the effect of making the dyke growing less
699 along the propagation direction and to develop crosswise. The propagation
700 velocity ratio, therefore, somehow inversely mimics the dyke breath ratio
701 between the vertical and the lateral phases.

4. Conclusions

702 Seismic observations contemporary to dyke propagation on basaltic vol-
703 canoes show stationary seismicity rate during dyke propagation in the last
704 phase before an eruption, despite possible variations of the dyke-tip velocity
705 [*Traversa and Grasso*, 2009]. Also, a clear and monotonic hypocenter mi-
706 gration of the seismicity contemporary to dyke propagation has been rarely
707 observed. These suggest that the observed dyke-induced seismicity is the re-
708 sponse of the edifice to the volumetric deformation induced by the magma in-

truding the solid matrix [*Traversa and Grasso*, 2009]. Accordingly, *Traversa and Grasso* [2009] argue for the stationary seismicity rate contemporary to the intrusion to be a proxy for a constant flux of magma entering the dyke in the unit time.

In order to test the implications of this assertion with respect to the volcano fluid dynamics, we implement a two-phase dyke propagation model, including a first vertical propagation followed by a lateral migration.

We demonstrate that, although propagation velocity varies of one order of magnitude among the different propagation phases (i.e. 1.3 $\mathrm{m\,s^{-1}}$ and 0.2 to 0.6 $\mathrm{m\,s^{-1}}$ for the vertical and lateral propagation, respectively), the flow rate of magma injected into the dyke can remain constant over time under given conditions. This is related both, to the fact that velocity depend on dyke size for the two propagation phases, and to the evolution of dyke growth, which is not limited only to elongation. It supports the idea of direct scaling between the magma flux intruding the solid and the observed seismicity rate through volumetric deformation. On the other hand it rejects a direct scaling between the seismicity rate and the dyke propagation velocity. In this sense the seismicity rate recorded at low-viscosity volcanoes during dyke intrusion represents the response of the solid matrix to a stationary volumetric deformation induced by the intrusion itself.

Obeying the laws governing fluid dynamics, the constant magma flux can be sustained by either, a constant or a slightly variable overpressure at the base of the dyke. The model we propose, however, does not allow for assert-

ing one hypothesis with respect to the other. Indeed it allows to investigate the implications of such a stationary flux hypothesis. For the vertical propagation, once the geometry and the physical parameters are fixed, the constant influx assumption bounds the range of possible initial magma overpressures and volumes of the magma reservoir. Specifically, only a magma reservoir with sufficiently small initial overpressure and sufficiently large volume is able to sustain a dyke injection fed at constant flux.

The flux value computed in the vertical phase is injected in the lateral propagation phase and it determines, together with static conditions of pressure equilibrium, dyke size and lateral propagation rate. In this way, the model we discuss in this paper allows to constrain the ratio between vertical and horizontal dyke thickness.

We validate the model in an application to the August 2003, Piton de la Fournaise eruption. It consists of two main phases: a vertical propagation, followed by a horizontal migration towards the eruption site [*Lénat and Bachèlery*, 1990; *Toutain et al.*, 1992; *Bachélery et al.*, 1998; *Bachélery*, 1999; *Peltier et al.*, 2005, 2007, 2008]. According to the classification proposed by *Peltier et al.* [2008], the August 2003 PdlF eruption is a so-called 'proximal' eruption, with eruptive activity concentrated on the volcano flank, close to the central cone.

In this framework, the small values of initial reservoir overpressure (i.e. $\leq$ 2.2 MPa), and the small variations of this overpressure accompanying dyke propagation (i.e. $\leq 6\%$) we obtain from the computation, argue for this

eruption to belong to an early stage of a PdlF refilling cycle [see *Peltier et al.*, 2008]. The small overpressure variations argue for either, the volume of magma withdrawn from the reservoir during the injection to be small compared to the reservoir volume, or the magma flow rate injected into the dyke in the unit time to be small compared to a possible continuous magma flow refilling the shallow reservoir from depth (as proposed by *Peltier et al.* [2007]).

The average intrusion velocities we compute for the dykes feeding the August 2003 PdlF eruption well reproduce the values estimated by *Peltier et al.* [2007] on deformation data basis. It further support the validity of our model.

In conclusion, the dyke propagation model we propose, allows for validating the constant magma influx initial condition as geophysically realist for volcano processes.

Acknowledgments. We thank B. Taisne and A. Peltier, for suggestions and interesting discussions. We aknowledge two anonymous reviewers for the care devoted to the review and the interesting and constructive remarks made. The data used in this study have been acquired by the Piton de la Fournaise Volcanological Observatory (OVPF/IPGP). Special thanks to V. Ferrazzini, in charge of the OVPF seismological network. P.T. and J.R.G. are supported by VOLUME-FP6 and TRIGS projects, contracts n. 08471 and 043386, respectively.

References

Aki, K., and V. Ferrazzini (2000), Seismic monitoring and modeling of an active volcano for prediction, *J. Geophys. Res*, *105*(B7), 16,617–16,640.

Aki, K., M. Fehler, and S. Das (1977), Source mechanism of volcanic tremor: fluid-driven crack models and their application to the 1963 Kilauea eruption, *J. Volcanol. Geotherm. Res*, *2*, 259–287.

Albarède, F. (1993), Residence time analysis of geochemical fluctuations in volcanic series, *Geochim. Cosmochim. Acta*, *57*(3), 615–621.

Aloisi, M., A. Bonaccorso, and S. Gambino (2006), Imaging composite dike propagation (Etna, 2002 case), *J. Geophys. Res*, *111*(B06404), doi:10.1029/2005JB003908.

Bachélery, P. (1999), Le Fonctionnement des volcans boucliers, Habilitation à Diriger des Recherches thesis, Univ. de la Reunion, Saint Denis, France, 698 pages.

Bachélery, P., P. Kowalski, P. Catherine, J. Delmond, P. Blum, and J. Croce (1998), *Precise Temporal and Mechanical Identification of Dyke Emplacement using Deformation Monitoring at Piton de la Fournaise.*, pp. 475 – 485, European Commission, EUR 18161 EN.

Battaglia, J., and K. Aki (2003), Location of seismic events and eruptive fissures on the Piton de la Fournaise volcano using seismic amplitudes, *J. Geophys. Res.*, *108*(B8), doi:10.1029/2002JB002193.

Battaglia, J., V. Ferrazzini, T. Staudacher, K. Aki, and J. Cheminee (2005), Pre-eruptive migration of earthquakes at the Piton de la Fournaise volcano

(Reunion Island), *Geophys. J. Int*, *161*(2), 549–558.

Carmichael, I., J. Nicholls, F. Spera, B. Wood, and S. Nelson (1977), High-Temperature Properties of Silicate Liquids: Applications to the Equilibration and Ascent of Basic Magma, *Phil. Trans. R Soc. Lond. A*, *286*(1336), 373–429.

Cornet, F. (1992), Fracture processes induced by forced fluid percolation, in *Volcanic Seismology, IAVCEI Proc. Volcanology*, vol. 3, pp. 407–431.

Einarsson, P., and B. Brandsdottir (1980), Seismological evidence for lateral magma intrusion during the 1978 deflation of the Krafla volcano in NE Iceland, *J. Geophys.*, *47*, 160–165.

Froger, J., Y. Fukushima, P. Briole, T. Staudacher, T. Souriot, and N. Villeneuve (2004), The deformation field of the August 2003 eruption at Piton de la Fournaise, Reunion Island, mapped by ASAR interferometry, *Geophys. Res. Lett*, *31*(14), L14,601.

Grasso, J., and P. Bachelery (1995), Hierarchical organization as a diagnostic approach to volcano mechanics: Validation on Piton de la Fournaise, *J. Geophys. Res.*, *22*, 2897–2900.

Ida, Y. (1999), Effects of the crustal stress on the growth of dikes: Conditions of intrusion and extrusion of magma , *J. Geophys. Res.*, *104*(B8), 17897–17909.

Klein, F., R. Koyanagi, J. Nakata, and W. Tanigawa (1987), The seismicity of Kilauea's magma system, *Volcanism in Hawaii*, *2*, 1019–1185.

Lahaie, F., and J. Grasso (1998), A fluid-rock interaction cellular automaton of volcano mechanics: Application to the Piton de la Fournaise, *J. Geophys. Res.*, *103*, 9637–9649.

Lénat, J., and P. Bachèlery (1990), Structure et fonctionnement de la zone centrale du Piton de la Fournaise, in *Le Volcanisme de La Réunion*, edited by J. Lénat, pp. 257–296, Centre de Recherches Volcanologiques, Clermont-Ferrand, France.

Lister, J. (1990a), Buoyancy-driven fluid fracture: the effects of material toughness and of highly viscous fluids, *J. Fluid Mech.*, *210*, 263–280.

Lister, J. (1990b), Buoyancy-driven fluid fracture: similarity solutions for the horizontal and vertical propagation of fluid-filled cracks, *J. Fluid Mech.*, *217*, 213–239.

Lister, J., and R. Kerr (1991), Fluid-mechanical models of crack propagation and their application to magma transport in dykes, *J. Geophys. Res.*, *96*(B6), 10049–10077.

Maaløe, S. (1998), Shape of ascending feeder dikes, and ascent modes of magma, *J. of Volcanol. Geotherm. Res.*, *81*(3-4), 207–214.

McKenzie, D. (1984), The Generation and Compaction of Partially Molten Rock, *J. Petrology*, *25*(3), 713–765.

Meriaux, C., and C. Jaupart (1998), Dike propagation through an elastic plate, *J. Geophys. Res.*, *103*, 18–18.

Mériaux, C., J. Lister, V. Lyakhovsky, and A. Agnon (1999), Dyke propagation with distributed damage of the host rock, *Earth Planet. Sci. Lett.*,

165(2), 177–185.

Muskhelishvili, N. (1963), *Some Basic Problems of the Mathematical Theory of Elasticity: Fundametal Equations, Plane Theory of Elasticity, Torsion and Bending*, Noordhoff.

Nercessian, A., A. Hirn, J. Lépine, and M. Sapin (1996), Internal structure of Piton de la Fournaise volcano from seismic wave propagation and earthquake distribution, *J. Volcanol. Geother. Res.*, *70*(3-4), 123–143.

Nishimura, T., S. Ozawa, M. Murakami, T. Sagiya, T. Tada, M. Kaidzu, and M. Ukawa (2001), Crustal deformation caused by magma migration in the northern Izu Islands, Japan, *Geophys. Res. Lett*, *28*(19), 3745–3748.

Pasteris, J. (1984), Kimberlites: Complex Mantle Melts, *Annu. Rev. Earth Planet. Sci.*, *12*(1), 133–153.

Pedersen, R., F. Sigmundsson, and P. Einarsson (2007), Controlling factors on earthquake swarms associated with magmatic intrusions; Constraints from Iceland, *J. Volcanol. Geotherm. Res.*, *162*(1-2), 73–80.

Peltier, A., V. Ferrazzini, T. Staudacher, and P. Bachèlery (2005), Imaging the dynamics of dyke propagation prior to the 2000–2003 flank eruptions at Piton de La Fournaise, Reunion Island, *Geophys. Res. Lett.*, *32*, L22,302.

Peltier, A., T. Staudacher, and P. Bachèlery (2007), Constraints on magma transfers and structures involved in the 2003 activity at Piton de La Fournaise from displacement data, *J. Geophys. Res.*, *112*(B03207), doi:10.1029/2006JB0004379.

Peltier, A., V. Famin, P. Bachčlery, V. Cayol, Y. Fukushima, and T. Staudacher (2008), Cyclic magma storages and transfers at Piton de La Fournaise volcano (La Réunion hotspot) inferred from deformation and geochemical data, *Earth Planet. Sci. Lett.*, *270*, 180–188.

Peltier, A., P. Bachèlery, and T. Staudacher (2009), Magma transport and storage at Piton de La Fournaise (La Réunion) between 1972 and 2007: A review of geophysical and geochemical data, *J. Volcanol. Geother. Res.*, *184*, 93–108.

Pinel, V., and C. Jaupart (2000), The effect of edifice load on magma ascent beneath a volcano, *Phil. Trans. R. Soc. A*, *358*(1770), 1515–1532.

Pinel, V., and C. Jaupart (2004), Magma storage and horizontal dyke injection beneath a volcanic edifice, *Earth Planet. Sci. Lett.*, *221*(1-4), 245–262.

Pitcher, W. (1979), The nature, ascent and emplacement of granitic magmas, *J. Geol. Soc.*, *136*(6), 627–662.

Prôno, E., J. Battaglia, V. Monteiller, J. Got, and V. Ferrazzini (2009), P-wave velocity structure of Piton de la Fournaise volcano deduced from seismic data recorded between 1996 and 1999, *J. Volcanol. Geotherm. Res.*, *184*(1-2), 49–62.

Roper, S., and J. Lister (2005), Buoyancy-driven crack propagation from an over-pressured source., *J. Fluid Mech.*, *536*, 79–98.

Rubin, A. (1993a), Dikes vs. diapirs in viscoelastic rock, *Earth Planet. Sci. Lett.*, *119*(4), 641–659.

888 Rubin, A. (1993b), Tensile fracture of rock at high confining pressure: impli-
889 cations for dyke propagation, *J. Geophys. Res.*, *98*(B 9), 15,919–15,935.
890 Rubin, A. (1995), Propagation of Magma-Filled Cracks, *Annu. Rev. Earth*
891 *Planet. Sci.*, *23*(1), 287–336.
892 Rubin, A., and D. Gillard (1998), Dike-induced earthquakes: Theoretical
893 considerations, *J. Geophys. Res.*, *103*(B5), 10,017–10,030.
894 Rubin, A., D. Gillard, and J. Got (1998), A reinterpretation of seismicity as-
895 sociated with the January 1983 dike intrusion at Kilauea Volcano, Hawaii,
896 *J. Geophys. Res.*, *103*(B5), 10,003–10,015.
897 Sapin, M., A. Hirn, J. Lépine, and A. Nercessian (1996), Stress, failure and
898 fluid flow deduced from earthquakes accompanying eruptions at Piton de
899 la Fournaise volcano, *J. Volcanol. Geotherm. Res.*, *70*(3-4), 145–167.
900 Shaw, H. (1980), The fracture mechanisms of magma transport from the
901 mantle to the surface, *Phys. Magmat. Proc.*, 201–264.
902 Sigmarsson, O., M. Condomines, and P. Bachèlery (2005), Magma residence
903 time beneath the Piton de la Fournaise Volcano, Reunion Island, from
904 U-series disequilibria, *Earth Planet. Sci. Lett.*, *234*(1-2), 223–234.
905 Spera, F. (1980), Aspects of magma transport, *Phys. Magmat. Proc.*, 265–
906 323.
907 Taisne, B., and C. Jaupart (in press, 2009), Dyke Propagation Through
908 Layered Rocks, *J. Geophys. Res.*
909 Tinard, P. (2007), Caractérisation et modélisation des déplacements du sol
910 associés a l'activité volcanique du Piton de la Fournaise, ile de la Réunion,

911 a partir de donées interférométriques. Aout 2003 - Avril 2007, Ph.D. thesis,
912 Université Blaise Pascal - Clermont-Ferrand II.

913 Toda, S., R. Stein, and T. Sagiya (2002), Evidence from the AD 2000 Izu
914 islands earthquake swarm that stressing rate governs seismicity, *Nature*,
915 *419*, 58–61.

916 Toutain, J., P. Bachelery, P. Blum, J. Cheminee, H. Delorme, L. Fontaine,
917 P. Kowalski, and P. Taochy (1992), Real time monitoring of vertical ground
918 deformations during eruptions at Piton de la Fournaise, *Geophys. Res. Lett*,
919 *19*(6), 553–556.

920 Traversa, P., and J. Grasso (2009), Brittle Creep Damage as the Seismic
921 Signature of Dyke Propagations within Basaltic Volcanoes, *Bull. Seismol.*
922 *Soc. America*, *99*(3), 2035-2043.

923 Villeneuve, N., D. Neuville, P. Boivin, P. Bachèlery, and P. Richet (2008),
924 Magma crystallization and viscosity: A study of molten basalts from the
925 Piton de la Fournaise volcano (La Réunion island), *Chemical Geology*,
926 *256*(3-4), 241–250.

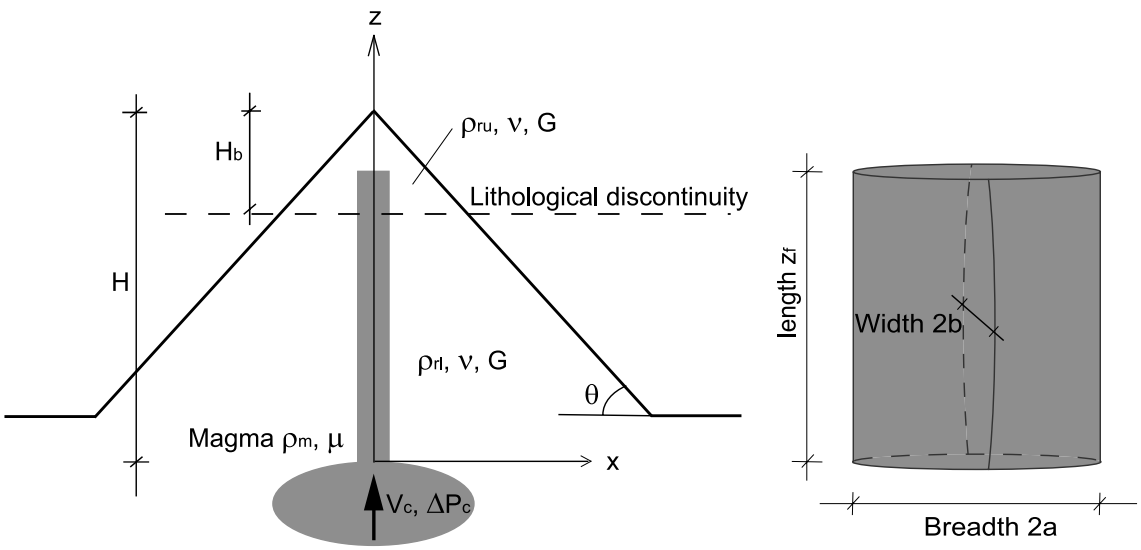

Figure 1. Sketch illustrating the geometry of a vertical dyke (left) and the shape of the fissure (rigth). $2\,b \ll 2\,a \leq z_f$. Half breadth a is assumed a priori.

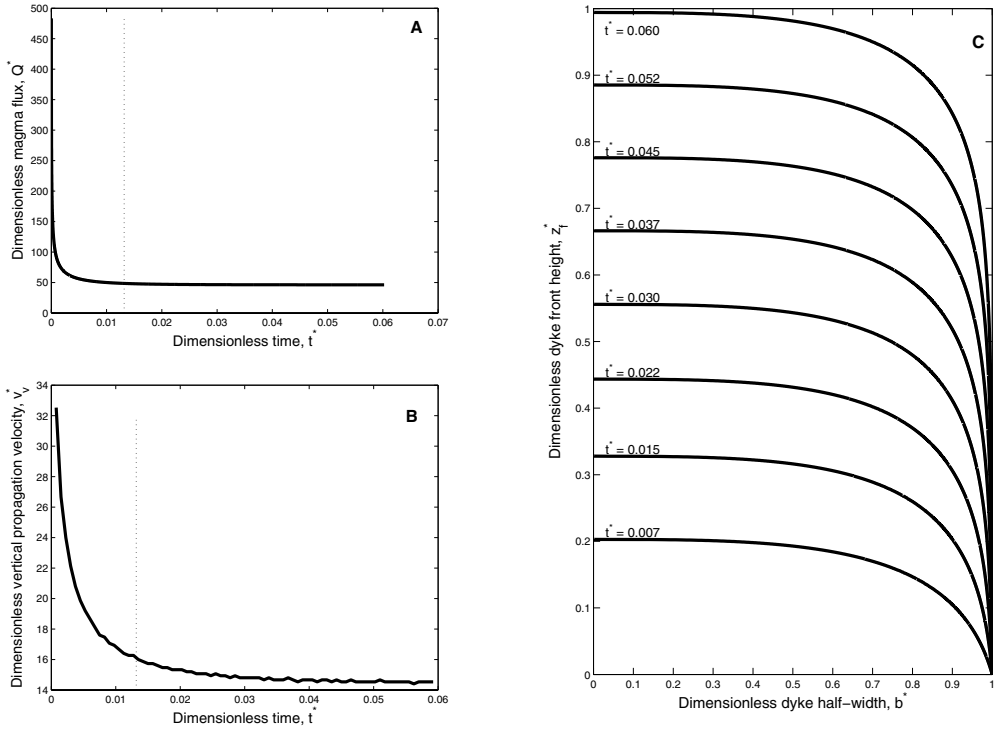

Figure 2. Magma-filled dyke rising in a homogeneous medium from a constant overpressure magma chamber at depth. A: dimensionless magma flux injected into the dyke over time; B: dimensionless propagation velocity versus time; C: Evolution of the crack shape for progressive growth stages. R_1 ($R_1 = (\rho_m - \rho_r)gH/\Delta P_0$) value used in the calculation is -3.55. Stipple-lines in plots A and B indicate $z_f^* = 0.3$. Reminder: $t = t^*[t]$, $Q = Q^*[Q]$, $v_v = v_v^*[v]$, $b = b^*[b]$, $z_f = z_f^*[H]$, where scales for time $[t]$, flux $[Q]$ and fracture width $[b]$ are given in equations (6) to (8), lengths are scaled by the reservoir depth H, and scale for propagation velocity is $[v] = [H]/[t]$.

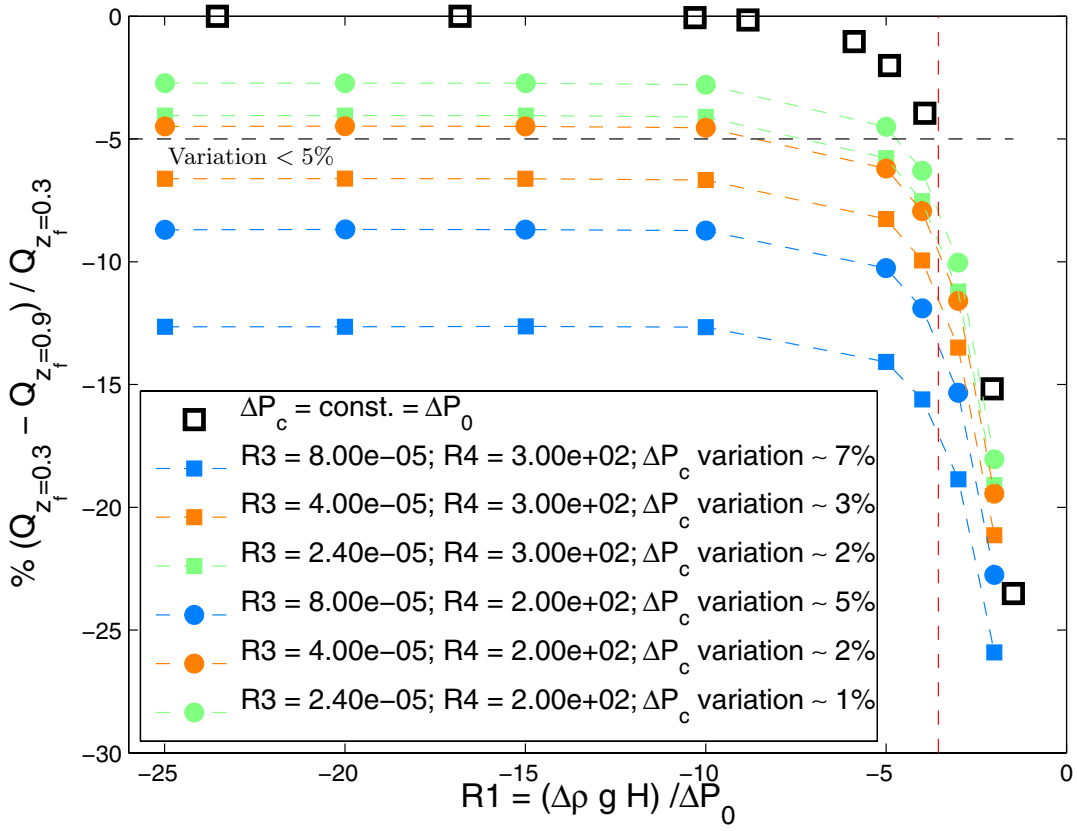

Figure 3. Percentage of magma influx variation during dyke growth within a homogeneous medium as function of the dimensionless number R_1 ($R_1 = (\rho_m - \rho_r)gH/\Delta P_0$). Black squares: constant overpressure at the dyke inlet; colored symbols: variable overpressure in the chamber. Color of solid symbols is related to the V_c value; circles or square symbols depend on the K value. Reservoir overpressure variations $\Delta P_c\, variation$ indicated in the legend are issued from the computation.

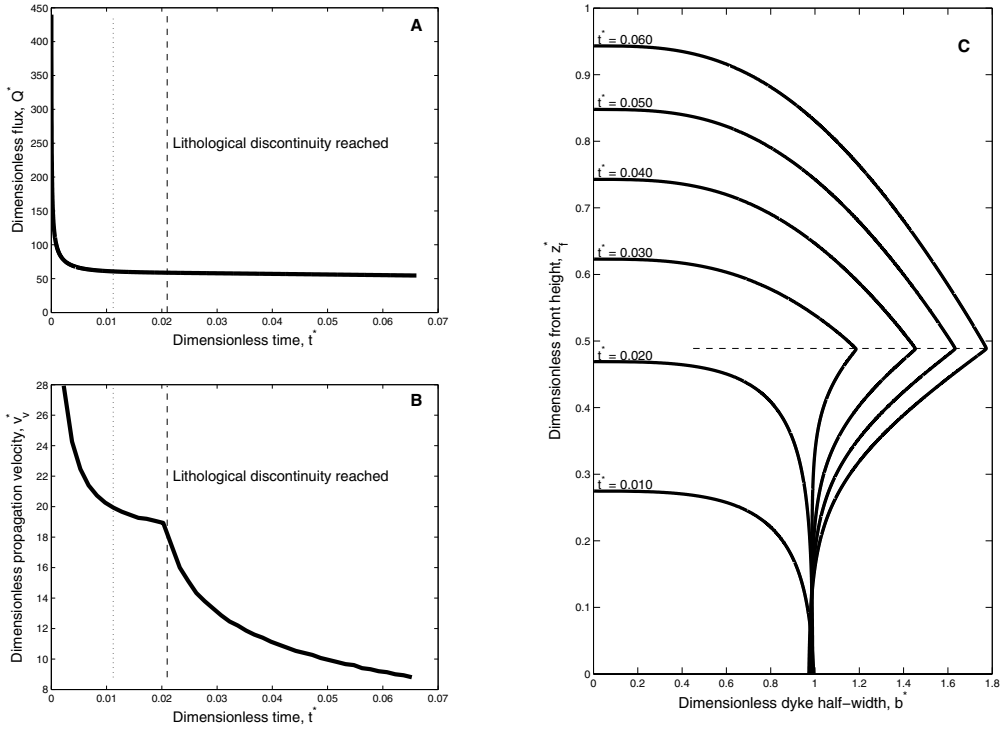

Figure 4. Magma-filled dyke rising in a homogeneous medium from a constant overpressure magma chamber at depth. A: dimensionless magma flux injected into the dyke over time; B: dimensionless propagation velocity versus time; C: Evolution of the crack shape for progressive growth stages. Parameter values used in the computation are: $R_{1l} = -4.82$, $R_{1u} = 1.37$, $R_2 = 0.51$, $R_3 = 6.9\text{x}10^{-9}$, $R_4 = 1.125$. Stipple-lines in plots A and B indicate $z_f^* = 0.3$. Reminder: $t = t^*[t]$, $Q = Q^*[Q]$, $v_v = v_v^*[v]$, $b = b^*[b]$, $z_f = z_f^*[H]$, where scales for time $[t]$, flux $[Q]$ and fracture width $[b]$ are given in equations (6) to (8), lengths are scaled by the reservoir depth H, and scale for propagation velocity is $[v] = [H]/[t]$; $R_{1u} = (\rho_m - \rho_{ru})gH/\Delta P_0$, $R_{1l} = (\rho_m - \rho_{rl})gH/\Delta P_0$, $R_2 = H_b/H$, $R_3 = (\Delta P_0\, a^2\,(1-\nu)\,H)\ (G\,V_c)$, $R_4 = 4KG/(\Delta P_0\,(4G+3K))$.

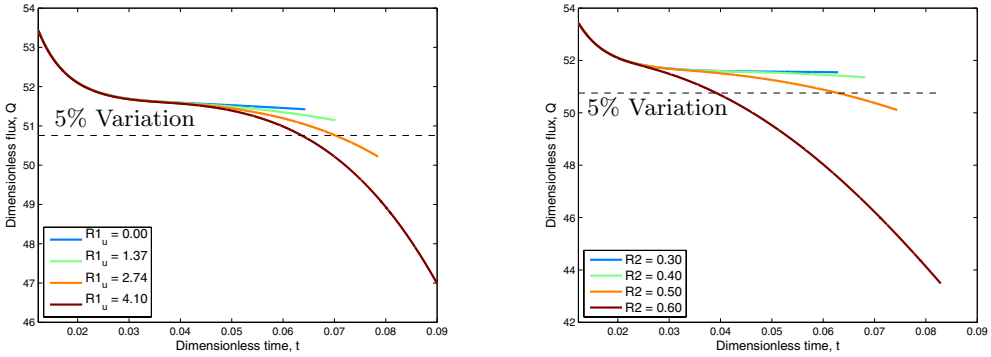

Figure 5. Left: effect of the dimensionless number R_{1ru} on the magma flux evolution over time during dyke propagation, $R_2 = 0.43$. Right: effect of the dimensioneless number R_2 on the magma flux evolution over time during dyke propagation, $R_{1ru} = 1.37$. For both cases $R_{1rl} = -4.1$, $V_c = 5\,\mathrm{km}^3$ and $K = 1\mathrm{x}10^9$ Pa. Final time corresponds to surface attainment. Reminder: $R_{1u} = (\rho_m - \rho_{ru})gH/\Delta P_0$, $R_{1l} = (\rho_m - \rho_{rl})gH/\Delta P_0$, $R_2 = H_b/H$, $R_3 = (\Delta P_0\, a^2\,(1-\nu)\,H)\;(G\,V_c)$, $R_4 = 4KG/(\Delta P_0\,(4G + 3K))$.

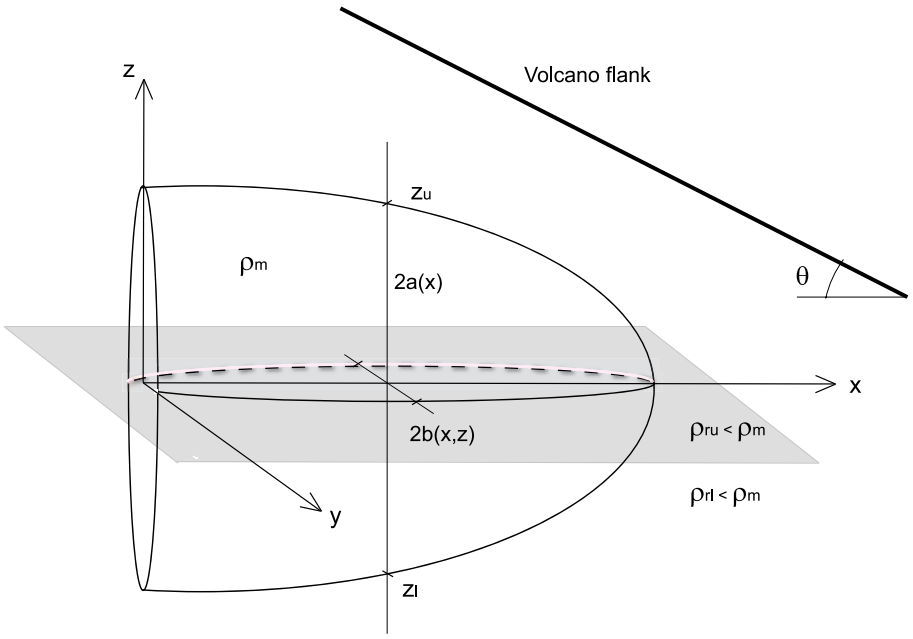

Figure 6. Sketch illustrating the geometry and the main parameters of a dyke horizontally propagating at the Level of Neutral Buoyancy

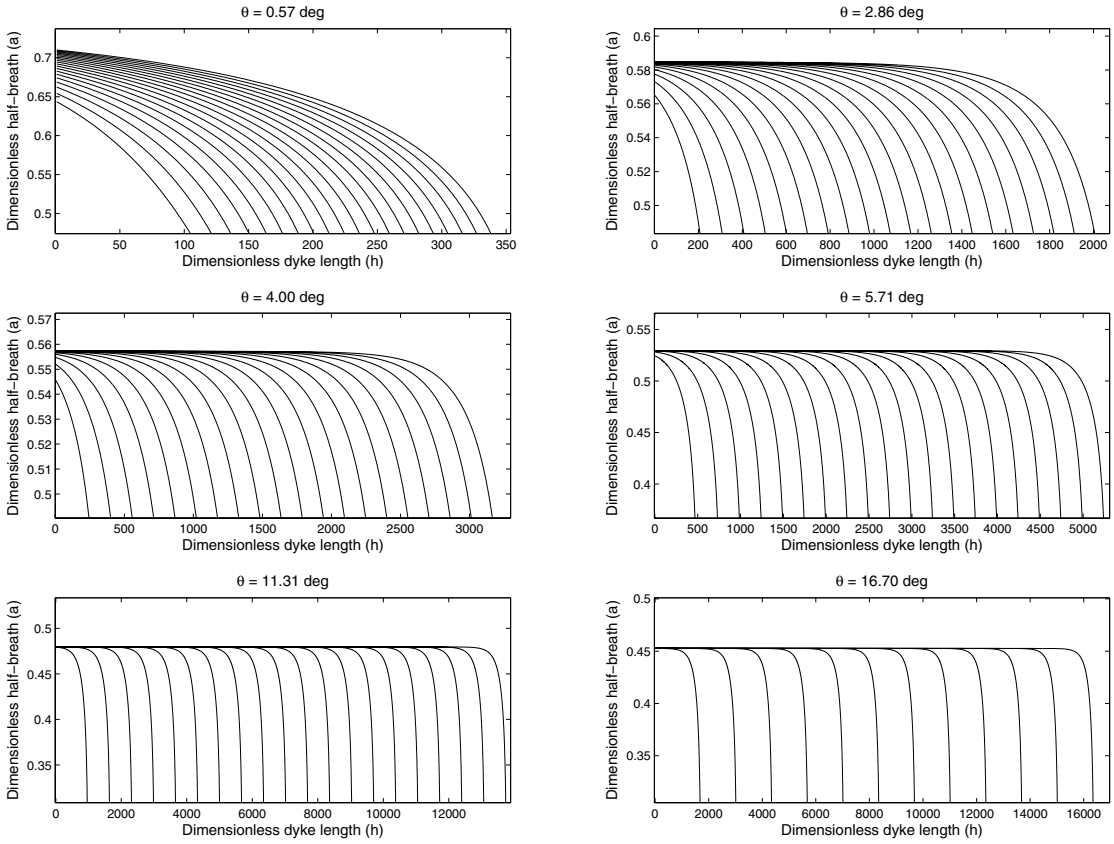

Figure 7. Lateral dyke propagation: effect of the edifice flank slope on the fracture shape evolution over time. Parameters used in the calculations are: $\rho_{rl} = 2700\,\mathrm{kg\,m^{-3}}$, $\rho_{ru} = 2300\,\mathrm{kg\,m^{-3}}$, $\rho_m = 2400\,\mathrm{kg\,m^{-3}}$. Dimensionless time step between following curves is 10^{-6}. Dimensionless numbers values are: $N_1 = 1.65\,\mathrm{x}\,10^{-4}$ and $N_2 = -1.48\,\mathrm{x}\,10^{8}$. Reminder: $N_1 = (3Q_{in}^{3/4}\mu^{3/4}G^{9/4})/(H_b^{9/4}(1-\nu)^{9/4}[P]^3)$, $N_2 = -(2H_b^3(1-\nu)^3[P]^4)/(3\mu Q_{in}G^3)$.

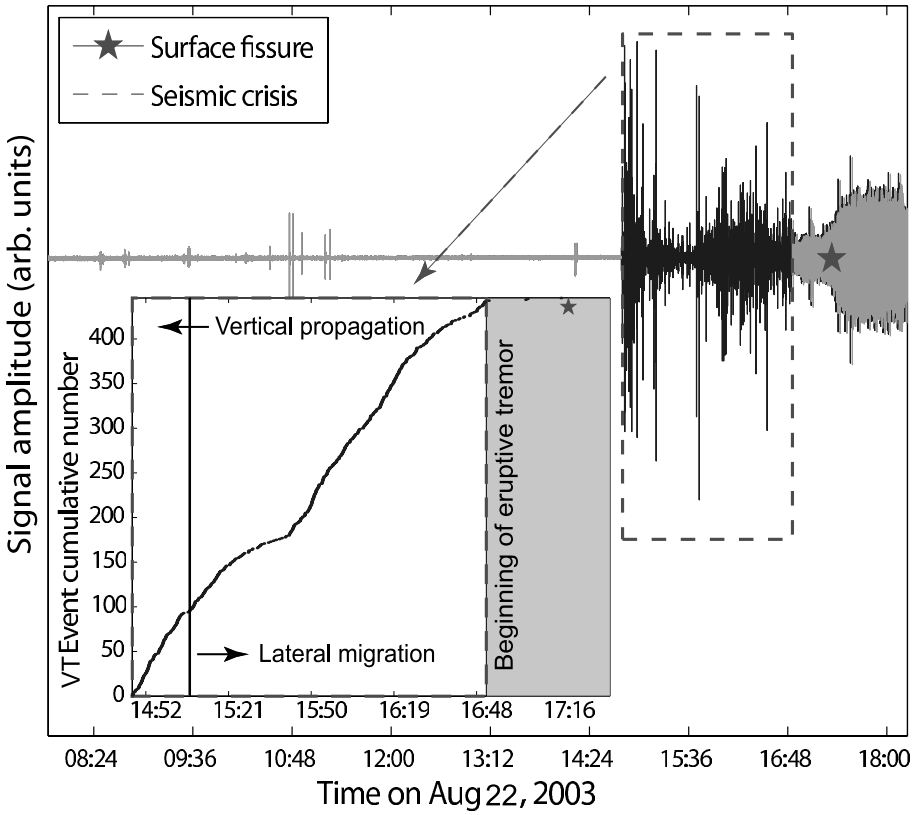

Figure 8. Seismic signal and cumulated seismicity (inset) hand-picked from continuous recordings recorded at the BOR summit station during the August 22 2003 dyke intrusion at Piton de la Fournaise volcano. Times related to the different stages of activity are from *Peltier et al.* [2007].

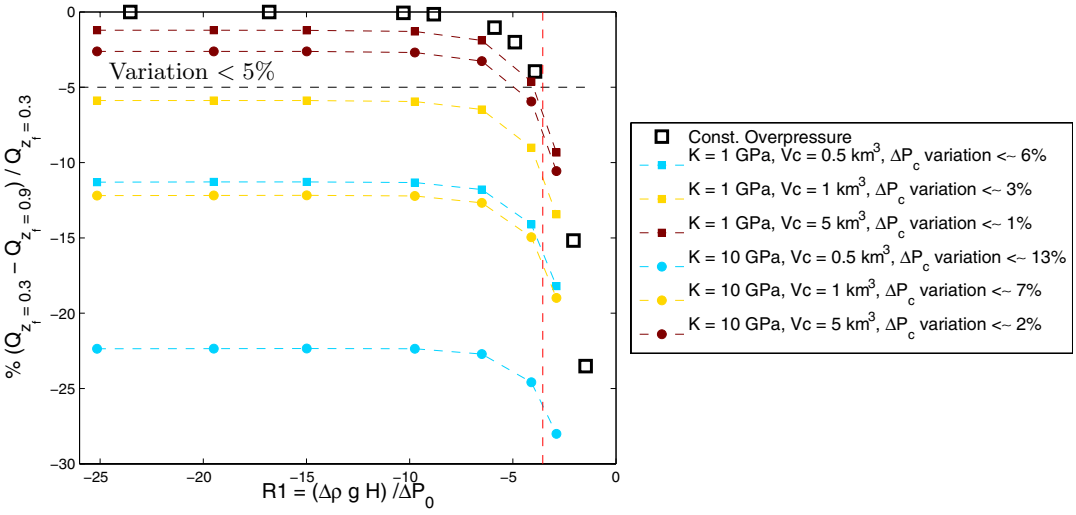

Figure 9. Interrelationship between magma influx and reservoir characteristics. Percentage of magma influx variation during dyke growth within a homogeneous medium as function of the dimensionless number R_1 ($R_1 = (\rho_m - \rho_r)gH/\Delta P_0$). Black squares: constant overpressure at the dyke inlet; colored symbols: variable overpressure in the chamber. Colors of plain symbols are related to the V_c value; circles or square symbols depend on the K value. Reservoir overpressure variations $\Delta P_c\, variation$ indicated in the legend are issued from the computation. Parameter values used are: $G = 1.125\text{x}10^9$ Pa, $\nu = 0.25$, $a = 100$m, $g = 9.81\,\text{m}\,\text{s}^{-2}$. V_c values derive from conceptual models of PdlF storage system [*Nercessian et al.*, 1996; *Sapin et al.*, 1996; *Peltier et al.*, 2007, 2008].

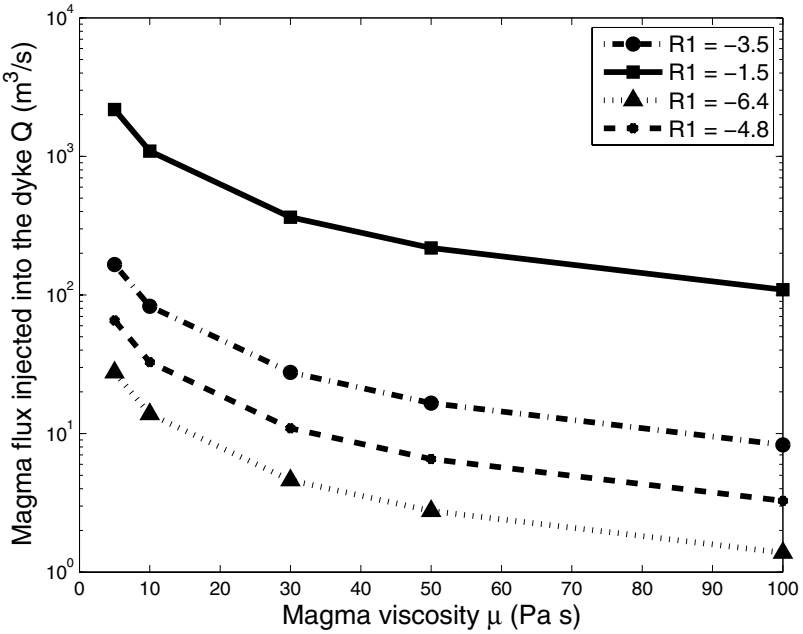

Figure 10. Dyke rising vertically within a homogeneous medium from a constant overpressure magma reservoir. Magma flux injected into the dyke as function of the magma viscosity and of the dimensionless number R_1 ($R_1 = (\rho_m - \rho_r)gH/\Delta P_0$). Parameters used are: $H = 2250$ m, $\rho_m = 2400$ kg m^{-3}, $\rho_r = 2750$ kg m^{-3}, $a = 100$ m, $\nu = 0.25$, $G = 1.125$ x 10^9 Pa.

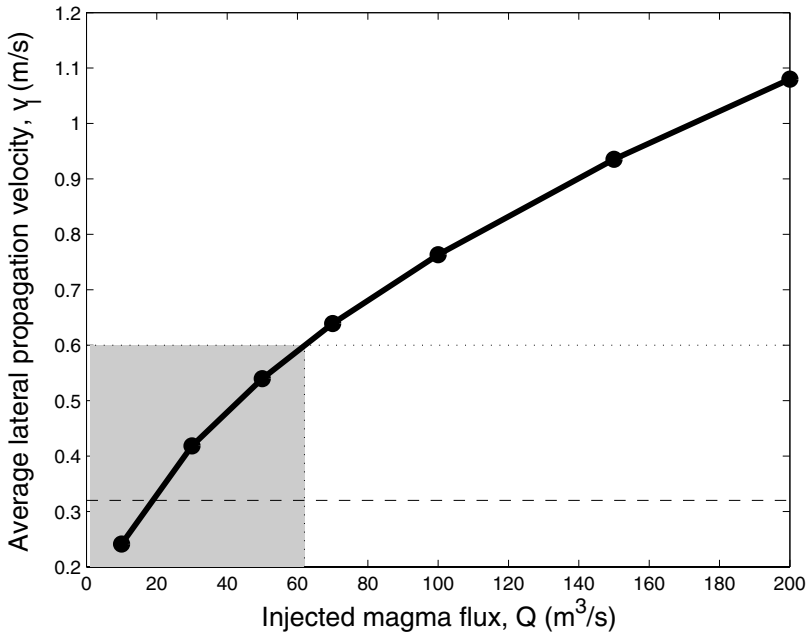

Figure 11. Lateral dyke propagation: average propagation velocity versus influx of magma injected into the dyke. Shaded area bounds the lateral propagation velocities estimated by *Peltier et al.* [2007] at Piton de la Fournaise. Parameters used are the following: $\theta = 11.8$ deg, $\rho_{rl} = 2750$ kg m^{-3}, $\rho_{ru} = 2300$ kg m^{-3}, $\rho_m = 2400$ kg m^{-3}, $H_b = 1150$ m, $G = 1.125$ x 10^9 Pa. Each magma flux value corresponds to a viscosity value, according to equation 39, where $A = 4.3936$ (from the vertical homogeneous case $R_1 = -3.55$). Reminder: $R_1 = (\rho_m - \rho_r)gH/\Delta P_0$.

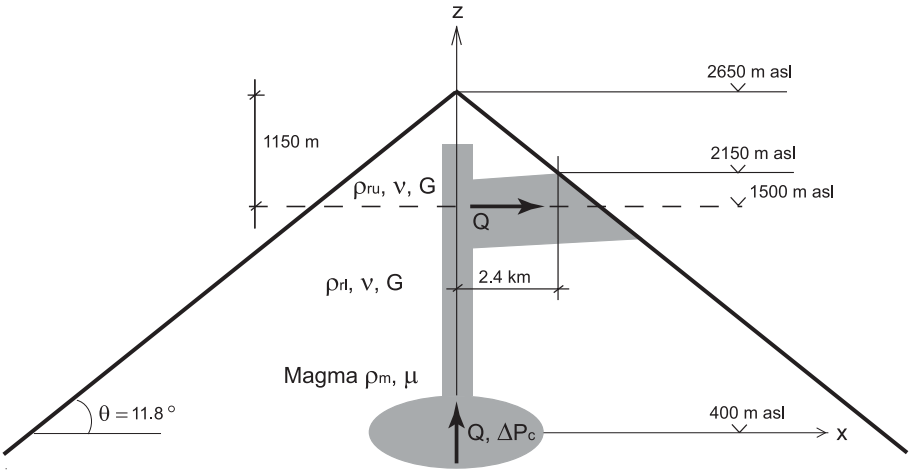

Figure 12. August 2003 PdlF case study. Sketch illustrating the geometry used in the model. Dotted line: input lithological discontinuity, position from *Peltier et al.* [2007]. Gray zones indicate magma path. All elevation data come from *Peltier et al.* [2007].

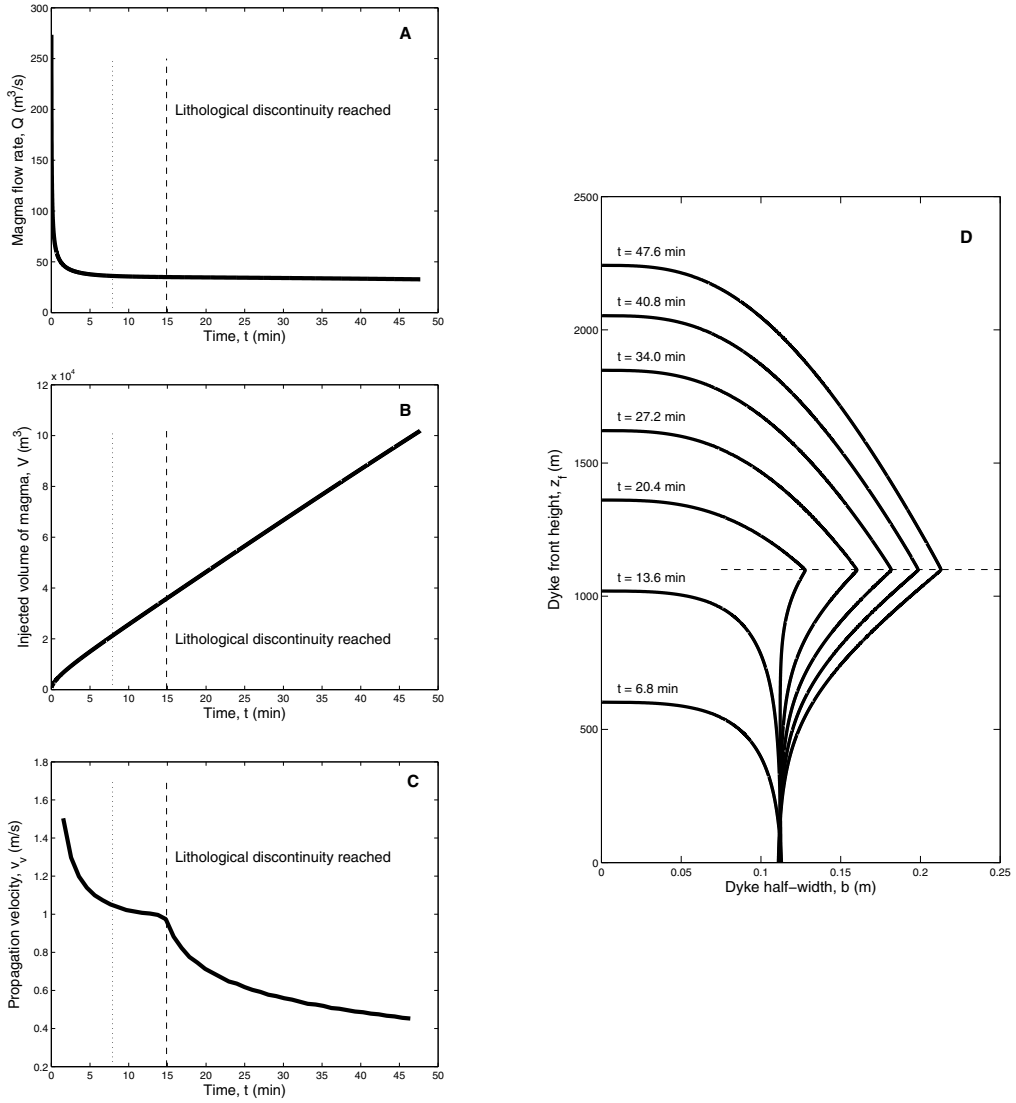

Figure 13. The effect of a lithological discontinuity on the vertical propagation of a magma-filled dyke. A: magma flux injected into the dyke over time; B: dyke volume (i.e. cumulative volume of magma injected into the dyke over time); C: propagation velocity versus time; D: Evolution of the crack shape for progressive growth stages. Parameter values used in the calculation are listed in table 2. Stipple-lines in plots A, B and C correspond to $z_f/H = z_f^* = 0.3$.

Table 1. Parameters used in the calculations for the case of a dyke rising in a homogenous medium from a large and fully compressible magma reservoir. †: from *Peltier et al.* [2007]; ‡: assumed parameters, as generic basalt values.

Parameter	Symbol	Value
Depth of the reservoir (m)†	H	2250
Poisson's ratio‡	ν	0.25
Shear modulus (Pa)‡	G	$1.125\text{x}10^9$
Rock density (kg m^{-3})‡	ρ_r	2750
Magma density (kg m^{-3})‡	ρ_m	2400

Table 2. Parameters used in the calculations applied to the August 2003 eruption at Piton de la Fournaise. †: parameter values estimated by *Peltier et al.* [2007]; ‡: assumed parameters as generic basalt values; § derived parameters; ⊛ parameter values from literature [e.g. *Lénat and Bachèlery*, 1990; *Nercessian et al.*, 1996; *Sapin et al.*, 1996; *Pinel and Jaupart*, 2000, 2004; *Peltier et al.*, 2008].

Parameter	Symbol	Value
Depth of the reservoir(m)†	H	2250
Half-length of the fracture(m)§	a	100
Poisson's ratio‡	ν	0.25
Shear modulus (Pa)‡	G	$1.125\text{x}10^9$
Rock density in the upper layer (kg m^{-3})‡	ρ_{ru}	2300
Rock density in the lower layer (kg m^{-3})‡	ρ_{rl}	2750
Depth of the lithological discontinuity (m)†	H_b	1150
Density of magma (kg m^{-3})‡	ρ_m	2400
Magma viscosity (Pa s)§	μ	11
Initial magma chamber overpressure (MPa)§:	ΔP_0	1.7
Edifice slope (deg)§	θ	11.8
Magma chamber volume (km^3)⊛	V_c	1.7
Magma bulk modulus (Pa)‡	K	$1\text{x}10^9$
Dimensionless numbers		
$R_{1l} = (\rho_m - \rho_{rl})gH/\Delta P_0$	R_{1l}	-4.54
$R_{1u} = (\rho_m - \rho_{ru})gH/\Delta P_0$	R_{1u}	1.30
$R_2 = H_b/H$	R_2	0.51
$R_3 = (\Delta P_0\, a^2\,(1-\nu)\,H)\ (G\,V_c)$	R_3	$1.5\ \text{x}10^{-5}$
$R_4 = 4KG/(\Delta P_0\,(4G+3K))$	R_4	352.90

Table 3. Model validation on the August 2003 Piton de la Fournaise eruption. Comparison between independent parameter estimations based on deformation data (from *Peltier et al.* [2007]) and computation results. *: [Peltier 2009, personal communication].

Parameter	Observation estimate	Model output
Vertical average dyke propagation velocity ($\mathrm{m\,s^{-1}}$)	$1.3 \pm 0.26^\star$	1.23
Lateral average dyke propagation velocity ($\mathrm{m\,s^{-1}}$)	$0.2 - 0.6 \pm 0.13^\star$	0.48
Lateral phase duration (min)	125	81
Lateral covered distance (m)	$2400 \pm 100^\star$	2300
Dyke total volume ($\mathrm{m^3}$)	$1 \pm 0.23^\star$ x 10^6	0.82 x 10^6